Petroleum Science 22 (2025) 1889–1911

Contents lists available at ScienceDirect

Petroleum Science

journal homepage: www.keaipublishing.com/en/journals/petroleum-science

Review Paper

Investigating petrophysical properties of gas hydrate-bearing sediments using digital rock technology: A microscopic perspective

Yang-Chen Fan [a, b], Wei-Chao Yan [a, b, c, *], Hui-Lin Xing [a, b, d], Xiu-Juan Wang [a, c], Huai-Min Dong [e, f], Xi-Mei Jiang [a, b], Ji-Lin Zhou [a]

[a] Frontiers Science Center for Deep Ocean Multispheres and Earth System, Key Lab of Submarine Geosciences and Prospecting Techniques, MOE and College of Marine Geosciences, Ocean University of China, Qingdao, 266100, Shandong, China
[b] International Center for Submarine Geosciences and Geoengineering Computing (iGeoComp), Ocean University of China, Qingdao, 266100, Shandong, China
[c] Laboratory for Marine Mineral Resources, Qingdao Marine Science and Technology Center, Qingdao, 266237, Shandong, China
[d] Laoshan Laboratory, Qingdao, 266237, Shandong, China
[e] School of Geological Engineering and Geomatics, Chang'an University, Xi'an, 710054, Shaanxi, China
[f] Xi'an Consin Energy Technology CO. LTD, Xi'an, 710100, Shaanxi, China

ARTICLE INFO

Article history:
Received 19 July 2024
Received in revised form
2 November 2024
Accepted 17 February 2025
Available online 19 February 2025

Edited by Meng-Jiao Zhou

Keywords:
Digital rock
Gas hydrate
Petrophysical properties
Numerical simulation

ABSTRACT

Natural gas hydrates are crystalline solid complexes with different morphologies found in marine sediments and permafrost zones. The petrophysical properties of gas hydrate-bearing sediments (GHBS) are crucial for understanding the characteristics of gas hydrate reservoirs, the spatial distribution of natural gas hydrates, and their exploitation potential. Geophysical exploration remains the primary approach for investigating the petrophysical properties of GHBS. However, limitations in resolution make it challenging to accurately characterize complex sediment structures, leading to difficulties in precisely interpreting petrophysical properties. Laboratory-based petrophysical experiments provide highly accurate results for petrophysical properties. Despite their accuracy, these experiments are costly, and difficulties in controlling variables may introduce uncertainties into geophysical exploration models. Advances in imaging and simulation techniques have established digital rock technology as an indispensable tool for enhancing petrophysical experimentation. This technology offers a novel microscopic perspective for elucidating the three-dimensional (3D) spatial distribution and multi-physical responses of GHBS. This paper presents an in-depth discussion of digital rock technology as applied to GHBS, with an emphasis on digital rock reconstruction and simulation of petrophysical properties. First, we summarize two common methods for constructing digital rocks of GHBS: petrophysical experimental methods and numerical reconstruction methods, followed by analyses of their respective advantages and limitations. Next, we delve into numerical simulation methods for evaluating GHBS petrophysical properties, including electrical, elastic, and fluid flow characteristics. Finally, we conduct a comprehensive analysis of the current trends in digital rock reconstruction and petrophysical simulation techniques for GHBS, emphasizing the necessity of multi-scale, multi-component, high-resolution 3D digital rock models to facilitate the precise characterization of complex gas hydrate reservoirs. Future applications of microscopic digital rock technology should be integrated with macroscopic geophysical exploration to enable more comprehensive and precise analyses of GHBS petrophysical properties.

1. Introduction

Natural gas hydrates are clathrate compounds that crystallize under the influence of van der Waals forces between water and gas molecules at low temperatures and high pressures. In nature, they are usually distributed in the ocean at depths ranging from 300 to 2100 m and in permafrost at depths of 0–900 m (Su et al., 2022; Chibura et al., 2022). Although estimates of global natural gas hydrate resources remain contentious, they are indisputably more abundant than those of conventional natural gas and shale gas

* Corresponding author.
E-mail address: yanweichao@ouc.edu.cn (W.-C. Yan).

https://doi.org/10.1016/j.petsci.2025.02.010

(Chong et al., 2016). Furthermore, each cubic meter of natural gas hydrate can release 164 m^3 of methane (CH_4) gas and 0.8 m^3 of water (Kvenvolden, 1995), with little pollution after combustion. Therefore, natural gas hydrates are distinguished by their high energy density, superior quality, and efficiency, making them a promising alternative clean energy source (MacDonald, 1990; Gajanayake et al., 2023). More than 30 countries and regions have conducted surveys and research on GHBS, and many countries, including the United States (the Alaska North Slope, the Gulf of Mexico), Canada (the Mackenzie Delta), Japan (the Nankai Trough), India (the Krishna-Godavari Basin, the Mahanadi basin), China (the Shenhu Area, the Qiongdongnan Basin), and South Korea (the Ulleung Basin), have developed long-term research and development plans aimed at ultimately achieving the commercial exploitation of gas hydrates (Ruppel and Collett, 2013; Collett et al., 2014; Zhu et al., 2021).

The petrophysical properties of GHBS, including electrical, elastic, and fluid flow characteristics, are crucial for the exploration and development of gas hydrates. These properties not only facilitate the identification of the most promising exploration areas but also improve the accuracy of reservoir behavior prediction during gas hydrate exploitation (Li et al., 2011; Kurihara et al., 2011; Guo et al., 2021, 2022a, 2022b). Geophysical exploration techniques, particularly seismic exploration, are widely employed to analyze the lateral and vertical petrophysical properties of hydrate-bearing regions, achieving resolutions at both kilometer and meter scales. The integration of well log analysis enables a more precise evaluation of the macroscopic petrophysical properties of GHBS (Zhang et al., 2022a; Yuan et al., 2021; Liang et al., 2022). However, owing to the intricate microstructure of GHBS, considerable variations may arise in rock porosity, hydrate saturation, permeability, and other parameters at different depths, despite similar geophysical exploration responses (Yuan et al., 2022). For instance, in coarse-grained hydrate-bearing sand layers, sediments with high clay content and high hydrate saturation can exhibit resistivity log values similar to those of sediments with low clay content and low hydrate saturation (Dong et al., 2022a, 2022b). The direct application of the traditional Archie's equation by researchers to calculate hydrate saturation may result in substantial errors in the evaluation of GHBS due to the similarity in resistivity values. As shown in Fig. 1, the magnified well log plot clearly shows that the saturation estimated by the digital rock model has a higher degree of correlation with the sample data (represented by black points) than that obtained using Archie's equation.

As a high-precision, small-scale technique, petrophysical experiments provide essential parameters for the exploration and exploitation of natural gas hydrates (Yuan et al., 2024; Li et al., 2012; Waite et al., 2009). Through laboratory measurements, researchers can more accurately predict the characteristics of hydrates under different conditions, including their stability under varying pressures and temperatures, as well as their interactions with the surrounding environment (Liu et al., 2017b; Li et al., 2023b, 2024; Zhao et al., 2023a). These measurements provide calibration references for geophysical exploration interpretations, thereby enhancing the accuracy of GHBS evaluations. In their analyses, advanced precision instruments and techniques are employed, including Raman spectroscopy, X-ray diffraction (XRD), X-ray computed tomography (X-CT), scanning electron microscopy (SEM), nuclear magnetic resonance (NMR), magnetic resonance imaging (MRI), and differential scanning calorimetry (DSC) (Zhang et al., 2017, 2020; Liu et al., 2017a; Kneafsey et al., 2010; Wu et al., 2018; Yang et al., 2017; Chen et al., 2012; Majid and Koh, 2024; Denning et al., 2022; Wells et al., 2021). These techniques enable a comprehensive study of the intrinsic properties of natural gas hydrates, as well as the fundamental petrophysical parameters of GHBS (Spangenberg and Kulenkampff, 2006; Winters et al., 2007; Gao et al., 2019). However, conducting experimental research on natural gas hydrates presents several challenges. In previous studies, hydrate synthesis experiments were often time-consuming due to the need for specialized high-pressure, low-temperature conditions. Notably, the latest advancements in hydrate synthesis technology have successfully reduced experimental durations to mere hours or even minutes (Zhang et al., 2022c; Xiao et al., 2023). Nevertheless, the substantial costs associated with the procurement and maintenance of experimental equipment, along with operational complexity, limit the widespread and continuous execution of experiments. Additionally, improper experimental procedures may result in unexpected hydrate decomposition, directly affecting the reliability of the results. These factors hinder the effective measurement and accurate characterization of petrophysical parameters associated with GHBS (Zhao et al., 2023b; Xing et al., 2022).

Over the past decade, digital rock technology has emerged as a widely adopted method for evaluating conventional oil and gas reservoirs, yielding substantial results, particularly in elucidating petrophysical properties from a microscopic perspective (Blunt et al., 2013). Digital rock technology encompasses two primary aspects: digital rock reconstruction and the simulation of petrophysical properties. The latter is performed using reconstructed digital rock models. The serial section tomography method (SSTM) (Tomutsa et al., 2007), laser scanning confocal microscopy (LSCM) (Shah et al., 2014), and X-ray CT scanning method (Liu et al., 2017a) are primary experimental techniques for 3D digital rock reconstruction, directly revealing rock microstructures. However, these techniques are subject to limitations related to experimental equipment, sample size, and scanning resolution. Numerical reconstruction methods can effectively reconstruct 3D digital rocks at a lower cost; however, their accuracy depends on the quality of input data and the algorithms employed (Ju et al., 2014; Tahmasebi et al., 2012; Øren and Bakke, 2002; Liu et al., 2009; Talukdar and Torsaeter, 2002; Yang et al., 2015). In summary, experimental methods yield high-resolution, authentic 3D images, making them ideal for research that requires precise structural details. However, they demand a substantial quantity of high-quality images to maintain the accuracy of 3D reconstructions. By contrast, numerical reconstruction methods, while potentially less precise, offer greater flexibility and cost-efficiency, making them well-suited for large-scale data processing and preliminary analyses. These methods rely on statistical information from a limited set of images, allowing for reasonable inferences and reconstructions with fewer images (Zhu et al., 2019; Chi et al., 2024; Wang et al., 2021). Furthermore, a variety of established simulation algorithms have been developed to assess different petrophysical properties of digital rocks (Zhao et al., 2013; Saenger et al., 2011; Ramstad et al., 2012; Talabi et al., 2009). Digital rock technology has achieved significant results in conventional oil and gas reservoir evaluations, enhancing confidence in their effective applications to GHBS. Currently, techniques such as CT, MRI, and SEM can reveal the microstructural characteristics of GHBS, making them crucial tools for accurate 3D reconstruction of digital rocks (Hiruta and Matsumoto, 2022; Lei et al., 2022a; Le et al., 2021). Additionally, numerical reconstructions have become key methods for studying the microstructural characteristics of GHBS due to their flexibility and multi-scale structure characterization capabilities (Dong et al., 2018a). With the advancements in numerical simulation techniques such as the finite element method (FEM), finite difference method (FDM), pore network modeling (PNM), and lattice Boltzmann method (LBM), these methods have been widely applied to study the petrophysical properties of GHBS (Garboczi, 1998; Roberts and Garboczi, 2002; Gerke et al., 2018; Huang et al., 2015; Qian et al.,

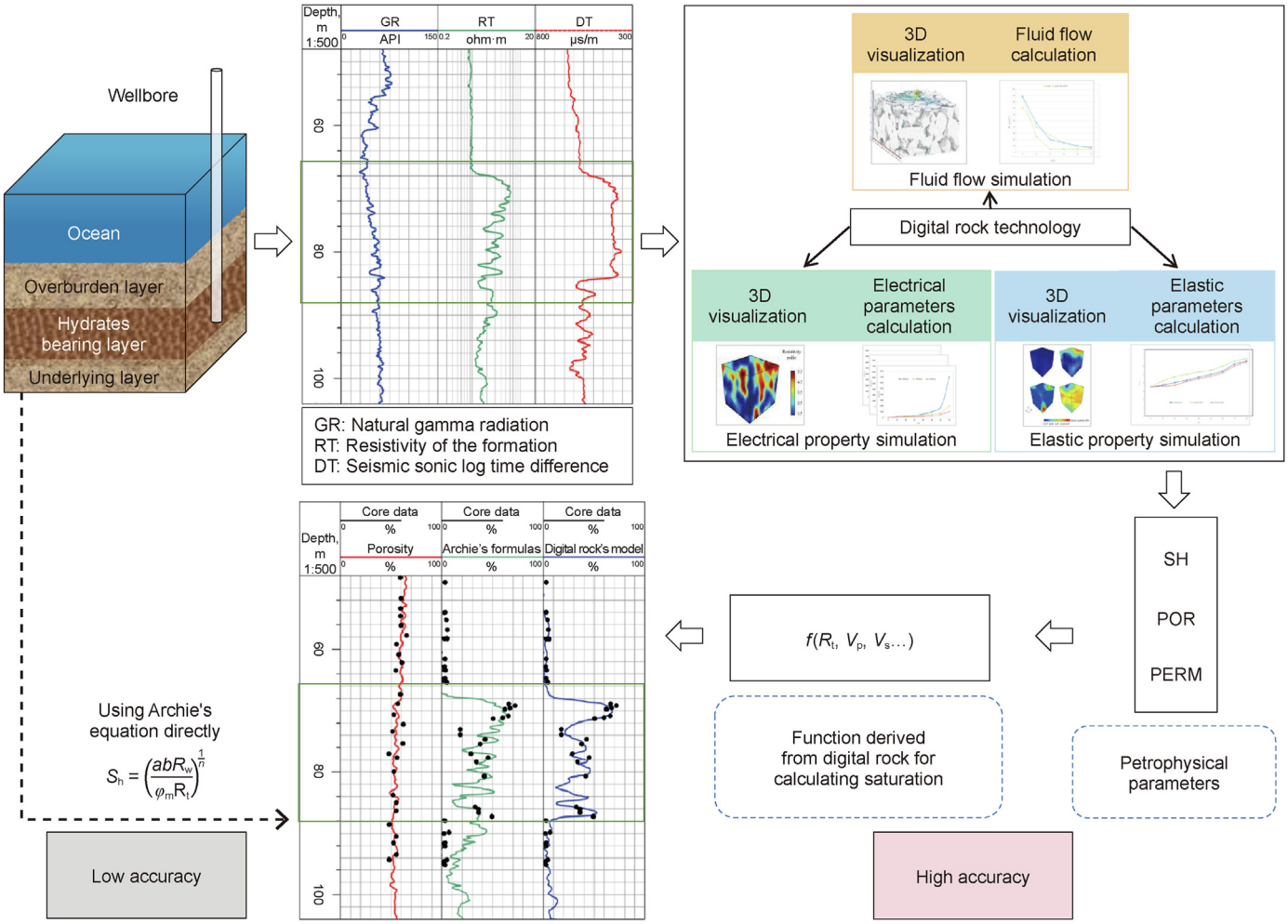

Fig. 1. The importance of digital rock technology in the geophysical exploration of GHBS.

1992). Consequently, as illustrated in Fig. 1, the critical role of digital rock technology in the geophysical exploration of GHBS lies in its capacity to optimize evaluation models derived from well log data, thereby reducing the uncertainty associated with reservoir parameters in well log interpretation. In our research, we summarize two commonly used methods for constructing hydrate-bearing digital rocks: petrophysical experimental methods and numerical reconstruction methods. The advantages and limitations of these techniques are also discussed. Using digital rock models of gas hydrates, we analyze methods for simulating the petrophysical properties of GHBS, including electrical properties, elastic properties, and fluid flow characteristics. Finally, by comprehensively reviewing current trends in digital rock construction and petrophysical property simulation from a microscopic perspective, we provide insights for accurately evaluating the petrophysical properties of GHBS across multiple scales.

2. Digital rock reconstruction methods

2.1. Experimental methods

The technique of acquiring two-dimensional (2D) rock images using advanced experimental equipment, such as X-ray CT, MRI, and SEM, followed by reconstructing these images into 3D models, is a widely adopted method for generating digital rock models.

2.1.1. X-ray CT

In the study of GHBS, X-ray CT scanning has become the primary method for digital rock reconstruction (Chaouachi et al., 2015). This technique employs X-ray scanners to perform non-destructive tomography on rocks, subsequently utilizing advanced computational processing technologies to reconstruct the acquired 2D images into 3D digital rock models. A significant advantage of this technique is its capacity to preserve the structural integrity of the rock, eliminating the need for sample destruction. Furthermore, the imaging data acquired through scanning provides comprehensive insights into the internal structure and delivers results regarding petrophysical properties.

Based on the source of the samples, CT studies of GHBS can be categorized into two groups. The first category comprises CT studies based on natural GHBS samples, while the second category includes CT studies based on artificial GHBS samples, as shown in Table 1. In 1992, Orsi et al. (1992) conducted research on marine GHBS using CT technology. They developed a method for preserving samples for imaging to capture the shape, internal structure, and orientation of natural gas hydrates within sedimentary environments. Subsequently, an increasing number of researchers have conducted CT scanning studies focusing on natural gas hydrates in permafrost and marine environments where hydrates are abundant. In the field of onshore permafrost research, Uchida et al. (2000) collected natural gas hydrate samples from the Mackenzie

Table 1
CT study of gas hydrates in natural GHBS samples and artificial samples.

Hydrate	Sample source/Composition	Remarks
Natural GHBS samples	The permafrost zone in the Mackenzie Delta	• The Mallik 2L-38 well has six gas hydrate forms, predominantly high-saturation CH_4 pore-space hydrates in sandy sediments (Uchida et al., 2000).
	The hydrate ridge in Oregon margin	• Hydrate Ridge has two gas hydrate types: shallow sediment-mixed hydrates and deeper fracture-filling hydrates (Abegg et al., 2007).
	The Ulleung Basin in the Sea of Japan (East Sea)	• Hydrates in veins, lenses, and nodules alter sediment shear and bulk stiffness (Yun et al., 2011).
	The NGHP–01 expedition in India and the Mount Elbert Stratigraphic Well on the North Slope of Alaska.	• Mount Elbert sandstone releases more gas after hydrate decomposition due to superior mechanical strength and permeability retention than NGHP-01 clay-rich cores (Kneafsey and Moridis, 2014).
	The Krishna–Godavari Basin, Bay of Bengal	• CH_4 mass balance and X-ray CT voxel intensity analysis yield similar hydrate saturation estimates, though CT values tend to be lower due to systematic errors (Holland and Schultheiss, 2014).
	The Green Canyon Block 955 in UT–GOM2–1 Expedition.	• Hydrate in silty sediments invades pores rather than displacing particles, forming a network, and altering mechanical properties (Lei et al., 2022a).
	The Umitaka Spur in the Sea of Japan	• Gas hydrates show varied morphologies, suggesting multi-stage growth and possible burial. Deformation signals imply lateral stress influence, complicating understanding in deeper sediments (Hiruta and Matsumoto, 2022).
	The Chapopote Asphalt volcano in the Gulf of Mexico	• SRXCTM analyzes natural gas hydrate microstructure, revealing crystallite size, pore networks, and connectivity, vital for modeling their petrophysical properties (Murshed et al., 2008).
Artificial GHBS samples	Ottawa sand; CH_4 hydrate	• Portable X-ray CT accurately tracks CH_4 hydrate dissociation dynamics in sediments, enabling precise measurement of distribution and decomposition (Freifeld and Kneafsey, 2004).
	Sand; CH_4 hydrate	• Microfocus X-ray CT effectively analyzes CH_4 hydrate sediment structure nondestructively under high pressure, accurately estimating porosity and hydrate saturation (Jin et al., 2006).
	Sand pack; Xe hydrate	• Ostwald ripening transitions hydrate from grain-attaching to pore-filling, affecting saturation heterogeneity and sediment properties (Chen and Espinoza, 2018).
	Ottawa sand; CH_4 hydrate	• CH_4 hydrate shifts from grain-attaching to pore-filling in sediments. Water/CH_4 gas presence influences pore-filling dynamics, impacting petrophysical properties (Lei et al., 2019b).
	Ottawa sand; Clay; CO_2 hydrate	• Factors such as clay content, P-T path, and initial sediment packing influence hydrate distribution. Nucleation and growth occur mainly at the core periphery due to heat dissipation and cryogenic suction (Lei et al., 2019a).
	Pure natural quartz sand; Natural quartz sand with a small quantity of montmorillonite clay particles; Glass beads; Xe hydrate	• Synchrotron-based microtomography reveals gas hydrate nucleation and growth patterns in sediments, emphasizing a vital fluid phase film between hydrates and quartz grains, crucial for interpreting seismic and transport properties (Chaouachi et al., 2015).
	Fontainebleau sand; CH_4 hydrate	• The study discovered unique CH_4 hydrate morphologies, like hollow filaments, and observed Haines jumps, indicating rapid water migration in sand pores (Le et al., 2021).
	Leighton Buzzard sand; CH_4 hydrate	• The study discovered the transition of hydrates from pore-floating to pore-bridging, culminating in the formation of an interpore hydrate framework (Sahoo et al., 2018).
	Leighton Buzzard sand; CH_4 hydrate	• The study revealed changes in gas bubble dynamics during CH_4 hydrate formation and decomposition, and how these changes significantly affect the geophysical properties of sediment (Madhusudhan et al., 2022).

Delta in northwest Canada, marking the first collection of such samples from the permafrost zone. With the assistance of CT scanning technology, researchers are able to visually characterize the morphology of natural gas hydrates in samples obtained from drilling sites. Despite the challenges inherent in microscopic-level research, this approach has effectively elucidated the distribution patterns of natural gas hydrates and solid grains. Considering the substantial reserves of natural gas hydrates in marine environments, researchers have increasingly focused on the study of samples collected from these locations. Abegg et al. (2007) collected hydrate samples from offshore Oregon in the western United States and preserved them in a foam box filled with liquid nitrogen. The structure of the frozen circular samples was analyzed using CT, revealing two predominant gas hydrate structures within the study area. This structural analysis suggests that the formation of gas hydrates is intricately linked to the host environment. Yun et al. (2011) recovered seven pressure cores from the Ulleung Basin. Subsequently, the samples were characterized using 2D and 3D images to analyze the spatial distribution of hydrates within the sediments. The pressure-temperature (P-T) stability conditions of the hydrates were maintained throughout the experimental process, thereby largely preserving the morphological distribution and petrophysical properties of the natural hydrate samples. Holland and Schultheiss (2014) evaluated gas hydrate saturation in offshore Indian pressure core samples using two methods: the mass balance of CH_4 collected after depressurization and the voxel intensity analysis of CT reconstructions. They found that the gas hydrate saturation measured by both methods was essentially equivalent. The CT intensity analysis method demonstrated the potential to estimate gas-liquid hydrate saturation in experimental samples, but it was unable to identify pore-filling gas hydrates. Future studies should consider testing pressurized rock samples using both quantitative techniques, comparing their accuracy, and comprehensively exploring possible errors. Lei et al. (2022a) selected samples from the northern Gulf of Mexico and conducted microscopic observations of gas hydrate pores under pressure-maintaining conditions. Throughout the sub-sampling and imaging process, the hydrates were maintained under stable pressure and temperature conditions. Fig. 2 illustrates a schematic of the multi-scale internal structure of GHBS. It presents hydrate images

generated by digital rock technology, including multiple scales from acquiring large-scale samples to reconstructing small-scale 3D models. The observations indicated that the hydrate phase in the pores of Gulf of Mexico sediments was pore-filling, with no cemented hydrates found. At the microscopic level, it is likely that the hydrates formed in these silty sediments are pore-intrusive rather than displacing particles. Furthermore, the hydrates may form continuous 3D networks, providing mechanical support to the sediment structure without directly cementing the particles.

In addition to conventional CT, synchrotron radiation X-ray cryo-tomographic microscopy (SRXCTM) offers a novel approach for scanning hydrates in a stable state. For example, Murshed et al. (2008) used SRXCTM to analyze samples collected from the Gulf of Mexico. The analysis focused on the porous network around the natural gas hydrate area, revealing characteristics by micron-scale boundary pores and larger pores within the frozen water phase. With technological advancements, there has been a growing trend toward high-resolution analyses of small-scale samples. However, the study of the overall morphology of GHBS remains limited. Hiruta and Matsumoto (2022) presented a comprehensive discussion on the application of CT technology for examining the overall morphology of GHBS. Their analysis of samples from the Umitaka Spur area revealed that the distribution of massive samples was non-uniform and consisted of a combination of multiple types of hydrates. Furthermore, the diversity in internal morphology observed in columnar samples further illuminated the complexity of their growth processes. Kneafsey and Moridis (2014) analyzed CH_4 hydrate samples from India NGHP-01 and the Mount Elbert area in Alaska using X-ray CT and experimental tests to investigate differences between frozen soil and marine hydrates. The study found that the NGHP-01 sample exhibited signs of hydrate decomposition during heating and depressurization, but no gas was released. In contrast, the Mount Elbert sample released gas successfully under similar conditions, and the numerical simulations corroborated the experimental data. They concluded that the gas exploitation potential of hydrate-bearing sand reservoirs exceeded that of clay reservoirs. This can be attributed to the deformation of the latter's structure following hydrate decomposition, which resulted in reduced gas mobility.

Natural GHBS are frequently challenging to acquire, and the gas hydrates contained within them are susceptible to decomposition during extraction and storage processes. As a result, artificial GHBS samples are more commonly used in studies of the microscopic characteristics of hydrates. Freifeld and Kneafsey (2004) conducted a series of experiments using artificial CH_4 hydrates in a sand matrix with a portable X-ray CT system, demonstrating the ability of CT imaging to track hydrate decomposition over space and time. The portability of the system allows for the field deployment of the measurement equipment, thereby avoiding challenges related to the preservation, storage, and transportation of CH_4-containing hydrate samples. Jin et al. (2006) conducted CT imaging of hydrate-containing sediments at 278 K and high pressure using a custom-built high-pressure reactor. Following gray-scale fitting, the spatial distributions of free gas, sand particles, water, and hydrates in the sediments could be clearly discerned. However, due to limitations in measurement accuracy, the microscopic distribution of hydrates was not directly observed but was instead determined through Gaussian fitting. Many researchers have used CT technology to study the formation and dissociation of artificial hydrates, allowing real-time monitoring of hydrate growth and decomposition (Kneafsey et al., 2007; Seol and Kneafsey, 2009). Chen and Espinoza (2018) conducted experiments on hydrates formed under three different conditions. They quantitatively assessed the isothermal growth rate and the Ostwald ripening process of hydrates using μCT technology, revealing their effects on the distribution of hydrates and pore-scale characteristics. This investigation offers a robust experimental foundation for comprehending the Ostwald ripening phenomenon of natural gas hydrates within

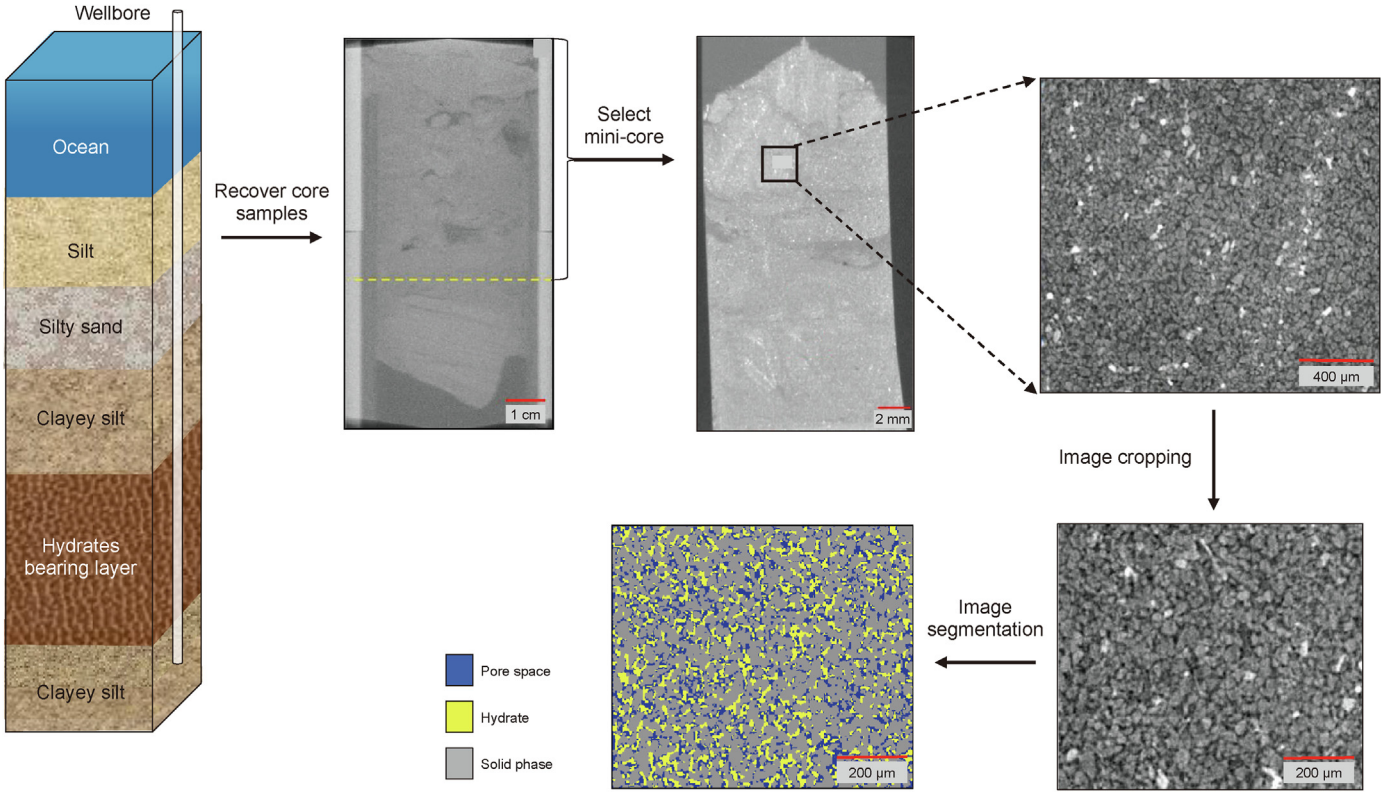

Fig. 2. Gas hydrate images at different scales (adapted with permission from Lei et al. (2022a)).

porous media. Lei et al. (2019b) utilized micro-CT to visualize the 3D pore behavior and evolution of CH_4 hydrate. A continuous sand filling experiment lasting 13 days was conducted under P-T conditions conducive to hydrate stability, demonstrating that the hydrate formation process is dynamic and involves significant material migration. The 2D sections and 3D visualizations during hydrate formation in the gas-excess system and the morphology evolution after brine injection are shown in Fig. 3. It is evident that hydrate formation progresses preferentially in confined directions instead of uniformly coating the particle surface. Lei et al. (2019a) employed CT to investigate the influence of fines content, the P-T path, and other factors on mass migration during the formation process of CO_2 hydrates. The experiment confirmed that water flowed to the periphery of the rock, with the hydrate preferentially crystallizing in a local spotty distribution while sediment particles moved toward the rock center. The freezing effect can promote water migration and particle movement, similar to the formation process of the hydrates. The P-T path and heat transfer rate directly determine the hydrate distribution in sediment during nucleation and growth. Chaouachi et al. (2015) reported the use of in situ synchrotron X-ray computed tomographic microscopy to observe the nucleation and growth of Xe-containing gas hydrates in various sedimentary matrices. Achieving a pixel resolution as high as 100 nm, this method offers a higher resolution than traditional CT, revealing finer microstructural changes. A comprehensive series of CT images documented the entire process of gas hydrate growth in the aqueous phase adjacent to quartz particles. Sahoo et al. (2018) also used synchrotron X-ray CT technology to study the evolution of CH_4 hydrate morphology in sediments and its influence on elastic wave velocity. They elucidated the transition of hydrates from pore-floating to pore-bridging, culminating in the establishment of an interpore hydrate framework. Additionally, they observed the coexistence of hydrates and gas, alongside the presence of a water film interposed between the hydrate and the sand. Madhusudhan et al. (2022) employed high-resolution synchrotron imaging and a convolutional neural network-based semantic segmentation technique to investigate the dynamic changes of gas bubbles during the formation and decomposition of CH_4 hydrates. They performed a detailed analysis of the morphological and dimensional changes of bubbles preceding and following hydrate formation, discovering that the distribution of bubble sizes significantly influences the geophysical properties of sediments. Synchrotron X-ray CT presents notable advantages in acquiring images of high spatial resolution. Nevertheless, its low temporal resolution may constrain the investigation of rapid interface evolution and complicate data interpretation. Optical microscopy, while providing superior temporal resolution (less than 1 s) for observing dynamic evolution, may be impeded by the opacity of particles. Le et al. (2021) attempted to combine these two types of pore-scale measurements, for the first time, combining high-resolution optical microscopy and synchrotron X-ray CT to observe the growth process of CH_4 hydrates in coarse sand sediments. This fusion method provides accurate images of CH_4 hydrate growth at the micron and subsecond levels, revealing the morphology and growth characteristics of CH_4 hydrate.

The utilization of CT technology in hydrate research continues to face two significant challenges: image resolution and component identification. The achievable image resolution with CT technology is constrained by several factors, including the performance characteristics of the CT equipment, scanning parameters, and sample dimensions. Consequently, when acquiring images of hydrate microstructures, researchers may encounter challenges related to low resolution, which hampers accurate identification and quantitative analysis of microscopic features. To mitigate this issue, certain researchers employ advanced instruments, such as synchrotron radiation X-ray CT, which yields high spatial resolution images with details below the micron scale (Kerkar et al., 2014; Alshibli and Jarrar, 2021; Nikitin et al., 2020; Yang et al., 2016). Nevertheless, the intricate technical principles and high-precision imaging capabilities necessitate sophisticated hardware and software, alongside expert operation and maintenance, resulting in elevated costs that restrict its wider application in research. The challenge of component identification primarily concerns the gas phase, liquid phase, and hydrates (solid phase), which may display similar density distributions and morphological characteristics in CT images, thereby complicating the identification process. Researchers commonly adopt two strategies to tackle these challenges. One involves adding soluble salts such as KI (Lei et al., 2018) and $BaCl_2$ (Chaouachi et al., 2015) to the pore liquid to enhance the contrast of the water phase. The alternative strategy utilizes Xe (Bian et al., 2022), CO_2 (Lei et al., 2019a), THF (Liu et al., 2019), and other guest molecules in hydrate experiments. Furthermore, certain researchers have explored the use of synthetic massive hydrates as markers within low-temperature and high-pressure vessels to facilitate comparisons with the actual hydrate phase, thus aiding in the precise localization and identification of hydrate phase boundaries (Hu et al., 2014). However, there are still limitations regarding how to ensure the stability of the markers during the operational transfer processes.

2.1.2. MRI

MRI technology can be used for investigating the formation and decomposition of natural gas hydrates, owing to its high spatial and temporal resolution. This technology enables the precise identification of the distribution of hydrates and non-hydrate phases, thus serving as an effective means of monitoring the dynamic processes of hydrate formation and decomposition (Baldwin et al., 2003).

THF and CO_2 hydrates, which are easily controllable in a

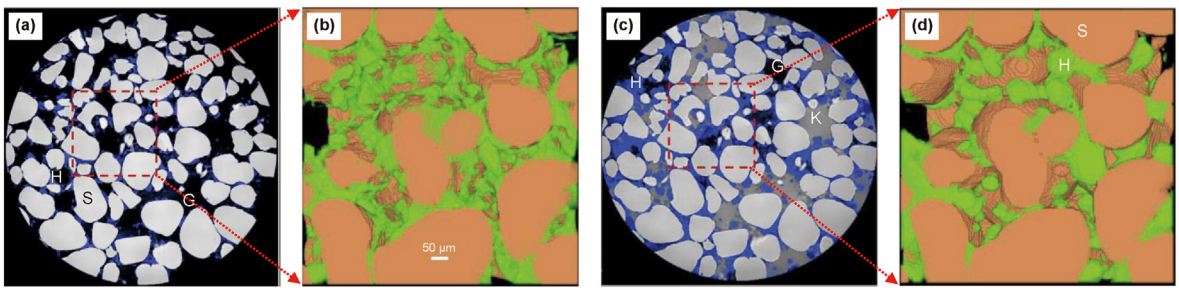

Fig. 3. Evolution of natural gas hydrate growth (adapted with permission from Lei et al. (2019b)). **(a)**–**(b)** 2D CT slice of sample 42–102 h after thermal spike (G = CH_4 gas, S = sand particle, H = CH_4 hydrate) and 3D CH_4 hydrate structure within the red area; **(c)**–**(d)** 2D CT slice of sample 54–114 h after KI solution injection (K = KI solution) and 3D CH_4 hydrate structure within the red area.

laboratory environment, are commonly used as substitutes. Mork et al. (2000) used MRI technology to explore the formation and decomposition of THF hydrate in sand layers, preliminarily revealing its behavioral characteristics in the undisturbed state, and verifying the feasibility of applying MRI technology to hydrate research under appropriate conditions. The hydrates in this study were generated under low-pressure conditions through the model system. The data obtained mainly demonstrated the distribution characteristics of the hydrates, without exploring the effects of pressure changes on their behavior. Zhao et al. (2011) utilized in situ MRI to observe the formation and dissociation of THF hydrate within quartz glass beads, thereby acquiring information on hydrate saturation at various time intervals. The research indicated that porous media possessing large specific surface areas and contact regions can promote the nucleation and formation of THF hydrates. During the growth process, crystals were observed to initially form on the glass beads, in their adjacent regions, as well as on the wall of the sample container. It was noted that nucleation accelerated with decreasing pore size or formation temperature. Additionally, it was found that the rate of hydrate dissociation primarily depended on the dissociation temperature rather than the pore size. Xue et al. (2012) conducted a study using MRI technology to monitor in real time the formation process of THF hydrates in porous media at different concentrations. Fig. 4 presents a series of cross-sectional images of hydrates changing over time in a 19% THF solution. In these images, the black regions denote glass beads and hydrates, whereas the white regions correspond to THF solutions that have not yet formed hydrates. The newly emerged black regions in the 65-min image signify the formation of THF hydrates. These images demonstrate that hydrates initially form at the contact points of particles, subsequently filling the entire pores, with growth exhibiting a stochastic pattern and reaching completion within 2 h. The study concluded that at higher concentrations, THF hydrates predominantly form cemented structures between media particles, whereas at lower concentrations, the hydrates tend to disperse freely within the pores. Kvamme et al. (2004) used MRI to monitor the phase transformation of CO_2 hydrate, and presented the experimental results of CO_2 hydrate formation and dissociation in real porous media. The 2D images indicated that hydrate growth occurred through nucleation rather than through the formation of discrete clumps. Similarly, Cheng et al. (2013) used MRI to closely observe the formation and dissociation processes of CO_2 hydrates in porous media. Their findings revealed that the growth rate and induction time of hydrates were influenced by the size of the porous media, the applied pressure, and the degree of supercooling. Based on these observations, the hydrate growth stage was categorized into the initial growth phase, the rapid growth phase, and the stable growth phase. During the growth stage, CO_2 hydrate initially formed on the container walls before gradually diffusing inward. In addition, it also tended to adhere to glass beads and occupy the pores. During the decomposition stage, the hydrate dissociation rate first increased to a maximum value, and then gradually decreased to zero.

Considering the differences in structure and properties between THF and CO_2 hydrates and natural gas hydrates, several researchers have attempted to use MRI to monitor the growth behavior of CH_4 hydrates in porous media. For example, Moudrakovski et al. (2004) detected the formation process of CH_4 and CO_2 hydrates in water droplets through ^1H magnetic resonance micro-imaging technology and analyzed the factors influencing the uneven hydrate formation in porous media. Bagherzadeh et al. (2011) studied the formation process of CH_4 hydrates in loose silica sand layers by using MRI, focusing on different grain size distributions and initial water saturations of sand grains to generate CH_4 hydrates. In these processes, the formation of hydrates was not uniform, and hydrate crystal nucleation occurred at different locations and times. They also observed that hydrates form more rapidly in a bed with lower water content and smaller grain size, but the underlying mechanisms still require further investigation. Zhang et al. (2019a) employed MRI to monitor the formation of CH_4 hydrates in media with varying levels of water saturation. They analyzed the characteristics of water and gas migration using both vertical and horizontal multi-slice samples. The results indicated that the vertical distribution of water molecules was primarily concentrated in the central region of the sample. As hydrates grew, the number of molecules in the central region and the surrounding regions exhibited a decreasing trend. Additionally, significant variations were observed in the hydrate formation processes across different horizontal slices. Noting that hydrate reformation and ice formation could occur during rapid depressurization and low-pressure

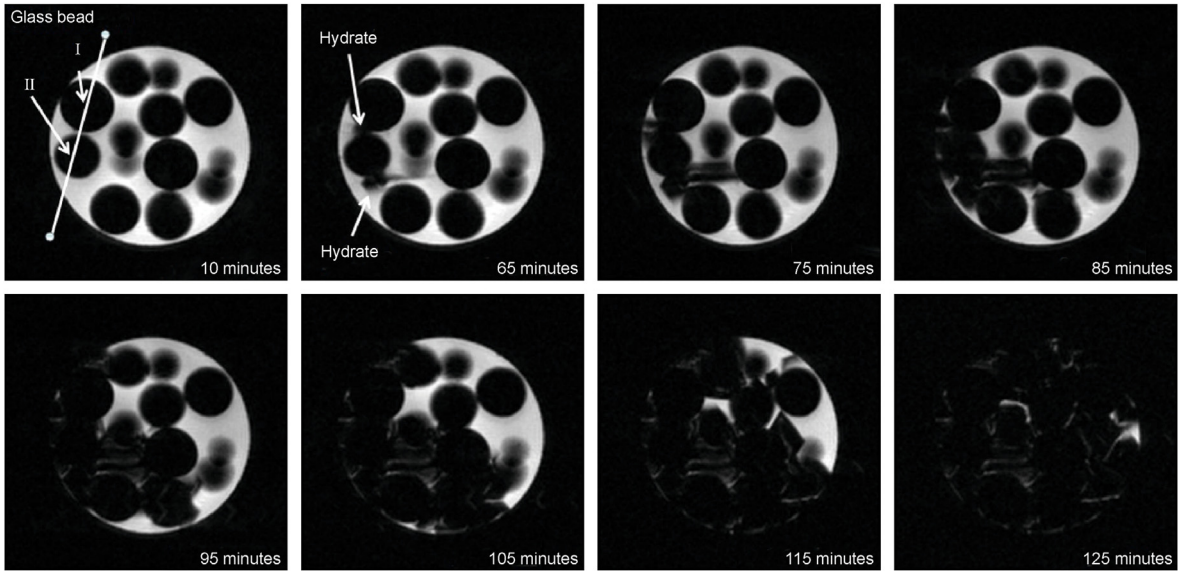

Fig. 4. Cross-section images of THF hydrate growth over time (reprinted with permission from Xue et al. (2012)).

production, Fan et al. (2017) conducted an MRI visualization analysis of the CH_4 hydrate dissociation process by gradually controlling the depressurization rate. Their focus centered on the ice formation under conditions of rapid depressurization and low back pressure, estimating the saturation of the ice formed within the container. While MRI can calculate hydrate saturation, phase difference, and pore size distribution, its limited resolution restricts the accurate characterization of GHBS structures.

2.1.3. SEM

Scanning electron microscopy (SEM) represents a high-resolution imaging technique that employs electron beams to elucidate the surface topography and structural information of samples. This technology has been widely applied in various fields, including materials science, biology, and geology (Echlin et al., 2020; Doshi et al., 2007).

With the rapid advancement of technology, our investigation into the microstructure of hydrates has reached unprecedented depths, making the application of SEM indispensable. As shown in Fig. 5, initial studies were primarily focused on the crystalline characteristics of CH_4 gas hydrates, examining their submicron-scale porous structures (Staykova et al., 2003). However, since 2007, researchers have increasingly concentrated on the submicron-scale pore details of actual hydrate samples, particularly the transition zones between the sub-micrometer-porous gas hydrate (SPGH) and the sediment (SED) dominated areas. In these transition zones, dense material (DM) appears intermittently, resulting in pores with diameters of several micrometers. Further observations reveal that in the transition from SPGH to DM, the single tube pores (T) exist in a hexagonal configuration, offering a new perspective for understanding the distribution characteristics of hydrates (Bohrmann et al., 2007). By 2014, researchers had elucidated the microstructural variations of natural gas hydrates and ice in samples through a series of sequential SEM images, providing insights into the morphological characteristics of natural gas hydrates under different environmental conditions. This finding was highly significant for distinguishing between these two substances (Stern and Lorenson, 2014). In 2022, through a comparative analysis of two distinct actual samples, researchers utilized SEM images to elucidate the pore structures and particle size characteristics of natural gas hydrate samples across various scales (Lei et al., 2022b). These findings not only enrich our understanding of microscopic hydrate structures but are also crucial for comprehending the storage characteristics and flow mechanisms of natural gas hydrates.

In the investigation of pore structural changes resulting from the formation and dissociation of hydrates, Lei et al. (2022b) conducted a detailed analysis using SEM on five unconsolidated samples from the hydrate bearing layer (HBL) and the underlying layer (ULL) in the Shenhu area of the South China Sea. The SEM results clearly revealed the internal pore structure and sedimentary particle morphology. Lu et al. (2022) utilized micro-CT and SEM to obtain digital images of three samples from the Shenhu area of the South China Sea and captured 2D nanoscale pore structure and mineral composition images using SEM. Utilizing these images, they analyzed the pore structure characteristics and mineral composition of the reservoir samples. To further investigate the surface characteristics of nanoscale hydrates in recovered samples,

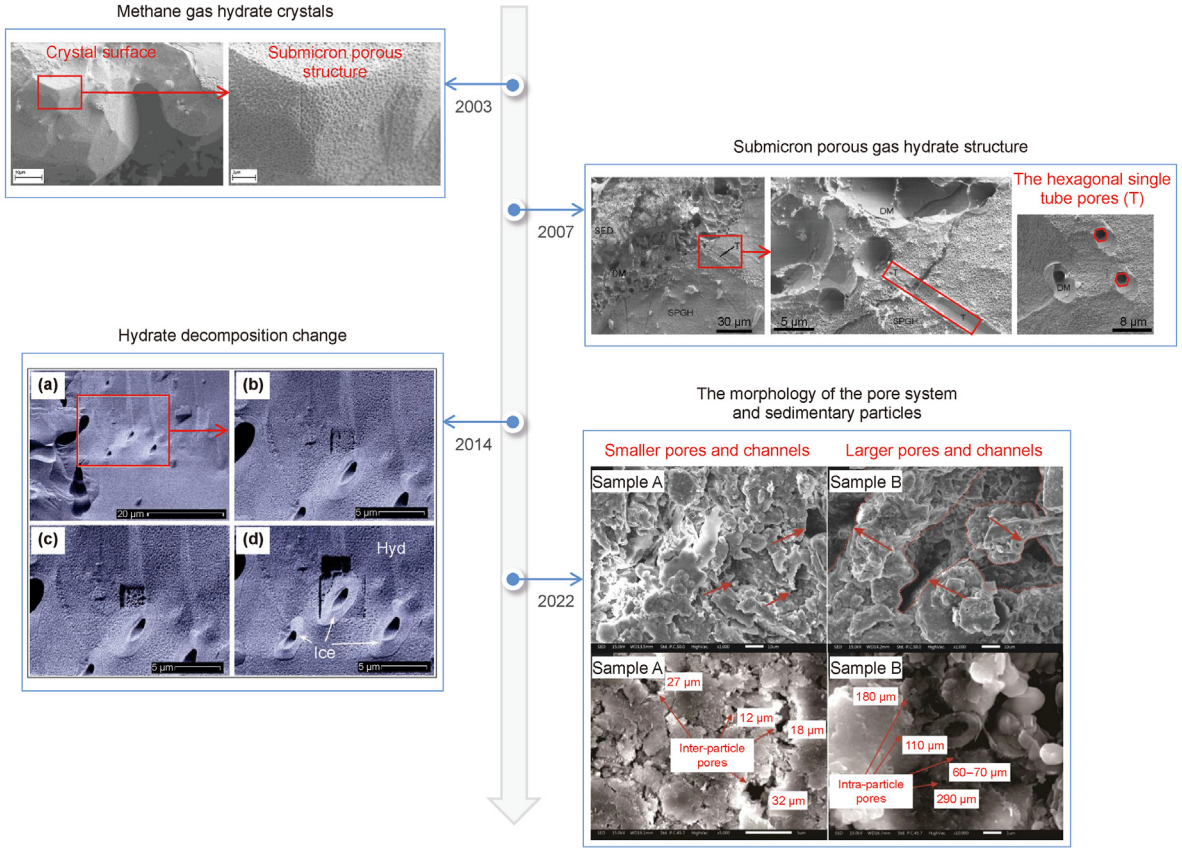

Fig. 5. SEM observation of gas hydrates (CH_4 gas hydrate crystals adapted with permission from Staykova et al. (2003). Submicron porous gas hydrate structure adapted with permission from Bohrmann et al. (2007). Hydrate decomposition change adapted with permission from Stern and Lorenson (2014). The morphology of the pore system and sedimentary particles adapted with permission from Lei et al. (2022b)).

some researchers integrated cryogenic sample chambers with SEM to establish cryogenic scanning electron microscopy (cryo-SEM), significantly enhancing the observation of natural gas hydrate pore spaces. Staykova et al. (2003) used cryo-SEM to observe submicron porous clathrates. Utilizing these observations, they constructed a phenomenological model that describes the kinetics of gas hydrate formation on ice powders, considering the effect of sample consolidation. Based on model simulations, multiple in situ kinetic neutron diffraction experiments were conducted to interpret the formation of CO_2 and CH_4 hydrates. Kuhs et al. (2004) integrated cryo-SEM technology with specific surface area measurements and discovered that the porosity of gas hydrates was primarily on the submicron scale and consisted mainly of closed pores. Efforts were undertaken to quantify the porosity of hydrates and correlate it with the observed macroscopic properties derived from image analysis. It was suggested that the submicron-scale porosity of gas hydrates significantly influences their petrophysical properties, particularly regarding their elastic characteristics.

Furthermore, several researchers have investigated the morphological structures and pore characteristics of gas hydrate samples retrieved from drilling cores at various locations, including the Oregon Margin, Southeast India Margin, Cascadia Margin, the Gulf of Mexico, and the Mackenzie River Delta, using cryo-SEM (Bohrmann et al., 2007; Stern and Kirby, 2008; Stern and Lorenson, 2014). Fig. 6(a) shows some gas hydrate samples from the Krishna–Godavari Basin off the east coast of India. Natural gas hydrate appears as bright white areas inside the nodule, ice appears as translucent gray, and marine silt and clay appear dark gray to black. Fig. 6(b) shows an SEM image of an area in the sample that has partially decomposed. Fig. 6(c) presents an SEM image of gas hydrate crystals in the sample, which are arranged on the inner wall of the pores and exhibit a fine crystal structure. This technology offers an effective method for evaluating the similarity between artificial and natural samples. Furthermore, the integration of X-ray diffraction with other analytical techniques facilitates the investigation of geological and geochemical influences on hydrate reservoirs. In order to gain a deeper understanding of the "self-preservation" phenomenon, Falenty et al. (2014) observed the time evolution of surface ice morphologies during CH_4 hydrate depressurization and decomposition using cryo-SEM and discussed how these morphologies affect the "self-preservation" efficiency. Sun et al. (2020) conducted a detailed analysis of both artificially created and naturally occurring natural gas hydrate samples using cryo-SEM. They discovered that different types of hydrates exhibited distinct surface morphologies; CH_4 hydrate (sI) had a smooth surface, whereas isobutane hydrate (sII) displayed a layered surface. The hydrates in the quartz sand were primarily characterized by pore-filling and the cementation of quartz sand. The natural hydrate-bearing samples were collected from the Shenhu area and the eastern Pearl River Mouth Basin in the South China Sea. The CH_4 hydrate occurred in massive and veined in the sediments. SEM observations revealed that the surface of these hydrates exhibits two main characteristics: one is dense and smooth, and the other is porous, which may be related to the supply rate of CH_4 gas.

However, this method may struggle to differentiate between ice and hydrates when they are in a frozen state, and it is easily limited during low-temperature preservation and recovery processes. Although cryo-SEM provides a means to capture structural details of GHBS, it is imperative to recognize the technical challenges associated with this technique. Additionally, SEM has its limitations, particularly in performing thorough and quantitative analyses of the pore structures of fine-grained sediments. To enhance the precision of pore structure characterization and behavior analysis in GHBS, a comprehensive approach that integrates multiple instruments and examines the subject across various scales and perspectives is essential.

2.2. Numerical reconstruction methods

The numerical reconstruction methods utilize image processing technology and numerical algorithms to extract information from 2D images and convert them into 3D models that accurately represent sediment structures. This approach offers the benefits of low cost and high efficiency, allowing for the fast generation of digital models on computers, which saves labor and material resources. Moreover, it provides the flexibility to reconstruct various types of digital rocks, making it convenient for investigating the properties of different rocks.

2.2.1. Constructing microscale digital rock models

While various methods exist for digital rock reconstruction, process-based methods are particularly favored for reconstructing digital rocks of GHBS. As early as 1985, Roberts and Schwartz proposed a method that simulated diagenetic processes, demonstrating the capability to depict a broad spectrum of porosities and grain systems characterized by both ordered and disordered structures (Roberts and Schwartz, 1985). However, this method primarily focused on the compaction process. Bakke and Øren (1997) proposed an innovative approach for creating 3D pore-scale models of both homogeneous and heterogeneous sandstones, known as the process-based method, which builds upon and enhances previous research. 3D digital rocks are constructed by simulating sedimentation, compaction, and diagenesis processes. The sedimentation simulation begins by extracting the grain size distribution from the sandstone image and randomly selecting grain sizes to generate sand grains. It then simulates compaction by adjusting the vertical axis while maintaining the shape of the sand

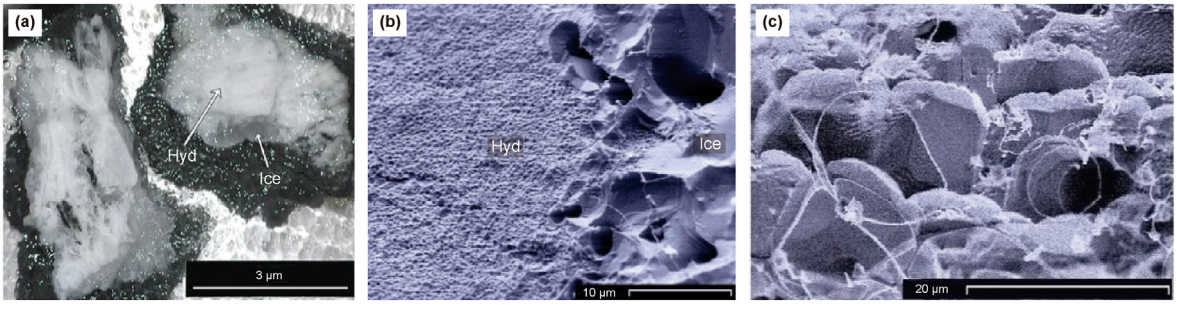

Fig. 6. Gas hydrate samples from Krishna–Godavari Basin (adapted with permission from Stern and Lorenson (2014)). **(a)** Photograph of natural gas hydrate samples; **(b)** SEM image at the hydrate-ice interface; **(c)** SEM image of natural gas hydrate crystals.

grains. Finally, the effects of diagenesis on rock properties are simulated through the simulation of quartz cementation and clay formation. Subsequently, Øren and Bakke (2002) applied this method to generate the 3D digital rock model of the Fontainebleau sandstone. A quantitative comparison between the experimental microstructure and the reconstructed model demonstrated that this method accurately replicated the geometric and conductivity properties of actual rocks. Furthermore, this method can construct 3D digital rock models with various hydrate cementation models, enabling an analysis of how these models affect rock properties (Dong et al., 2018a; Dong, 2020). In their study of the Mallik gas hydrate, Mohammadmoradi and Kantzas (2018) considered the granularity and looseness of the sediments in the area. Using geological information such as grain distribution and porosity, they employed the swelling ball algorithm to reconstruct porous media with spherical grains. The resulting sandy microstructure exhibited characteristics akin to those of Mallik sediment types, laying the groundwork for the investigation of reservoir petrophysical properties. Fig. 7 illustrates digital rock models produced by the process-based method with varying mean grain radii. Blue represents pores, and gray represents the solid matrix. The figure clearly demonstrates that under the identical porosity conditions, different grain sizes result in significant variations in sediment pore radii; similarly, under the constant grain size, hydrate-bearing sediments with varying porosities can be generated.

2.2.2. Hydrate distribution simulations

Understanding the occurrence of GHBS is crucial for elucidating the formation mechanisms, exploration strategies, and resource assessment of natural gas hydrates. Numerous theoretical models have been proposed by researchers to examine the influence of occurrence patterns on the petrophysical characteristics of gas hydrates.

Dvorkin et al. (2000) proposed three growth models of hydrates while studying the acoustic velocities of sediments containing hydrates: suspended, supporting, and cemented. Dai et al. (2004) identified six occurrence patterns in their study of elasticity and gas hydrate saturation: cemented, grain-coating, supporting, pore-filling, matrix and inclusions, and nodules/fracture-filling. Supporting and pore-filling hydrates are considered variants of the cemented model, where hydrates act as components of the load-bearing matrix or pore fillers. In contrast, the matrix and inclusion model treats gas hydrates and particles as the matrix and inclusions, respectively. Nevertheless, empirical evidence from actual rock samples indicates that hydrates predominantly manifest as nodules/fracture-filling structures in shallow argillaceous sediments, necessitating the application of the nodules/fracture-filling model for accurate characterization. Mahabadi et al. (2019) proposed a patchy occurrence pattern in the experiment studying the effect of hydrate saturation on the permeability of hydrate-containing sediments. The patchy occurrence pattern refers to hydrates that have undergone Ostwald ripening under pore-filling conditions. Dai et al. (2012) demonstrated through experimental data and petrophysical analysis that hydrates in hydrate-bearing sands exhibit a heterogeneous, patchy distribution, characterized by zones of 100% hydrate saturation within pore spaces that are embedded in hydrate-free sand. Considering the patchy distribution of hydrates allows for more precise estimations of the petrophysical properties of hydrate-bearing sands, as well as the investigation of the correlation between hydrate saturation and these properties. Hu et al. (2014) used CT to investigate the microscopic distribution and evolution of hydrates within the pore space of sediments. The results showed that hydrate distribution patterns at various saturation stages displayed mixed characteristics. Throughout the different stages of hydrate formation, distinct distribution patterns predominated. Contact or cementation models dominated in the early synthesis stages; suspension models were more common in intermediate stages; and suspended aggregation and re-cementation were prevalent in the late stages. We have summarized common microscopic occurrence patterns for GHBS, based on prior research, as shown in Fig. 8.

To enhance our comprehension of the formation mechanisms of hydrates and their impact on petrophysical properties, we can utilize digital rock technology to generate rock models containing hydrates. The first step involves constructing a realistic pore skeleton structure, followed by simulating the distribution of hydrates within the pore space. To enhance authenticity, many studies employ CT or other imaging technologies to acquire 3D images of the sample and then apply image processing and segmentation algorithms to extract the geometry and dimensions of the pore space, thereby constructing a realistic pore skeleton structure. Various simulation methods currently exist for modeling the diverse distribution patterns of hydrates. Liu et al. (2020) used a random nucleation and growth method to generate three types of hydrate occurrence with varying saturation levels, including pore-filling, patchy, and particle-coating, in 2D digital samples. During the simulation of hydrate nucleation and growth, distance checks are performed between all pore pixels, updating potential nucleation sites before converting any pore pixel into a hydrate pixel. Their simulation assumes no interface tension, thus eliminating limitations on hydrate growth due to heat and mass transfer constraints. Fukumoto et al. (2017) developed a numerical model that integrates classical nucleation theory and the phase-field model to predict the microscopic distribution of CH_4 hydrates in sand sediments. The model determines the locations of hydrate nucleation using classical nucleation theory and simulates the growth process

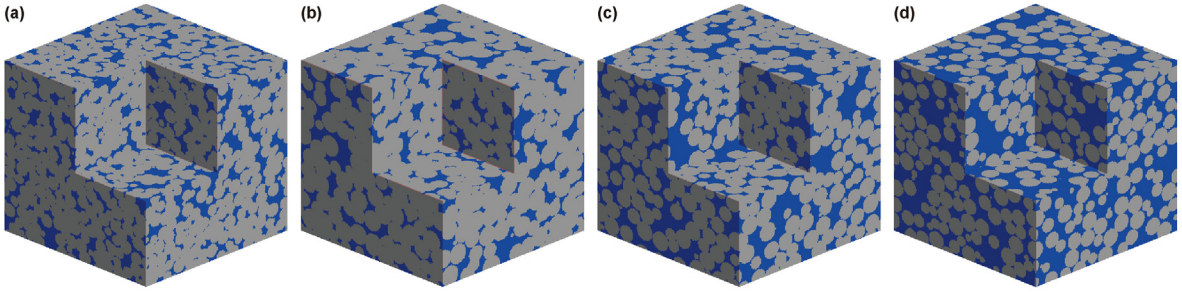

Fig. 7. Digital rock models generated using the process-based method. In **(a)** and **(b)**, both models have a porosity of 20% with grain radii of 70 μm and 100 μm, respectively. In **(c)** and **(d)**, both models feature grain radii of 100 μm and porosities of 30% and 40%, respectively. Blue represents pores, and gray represents the solid matrix.

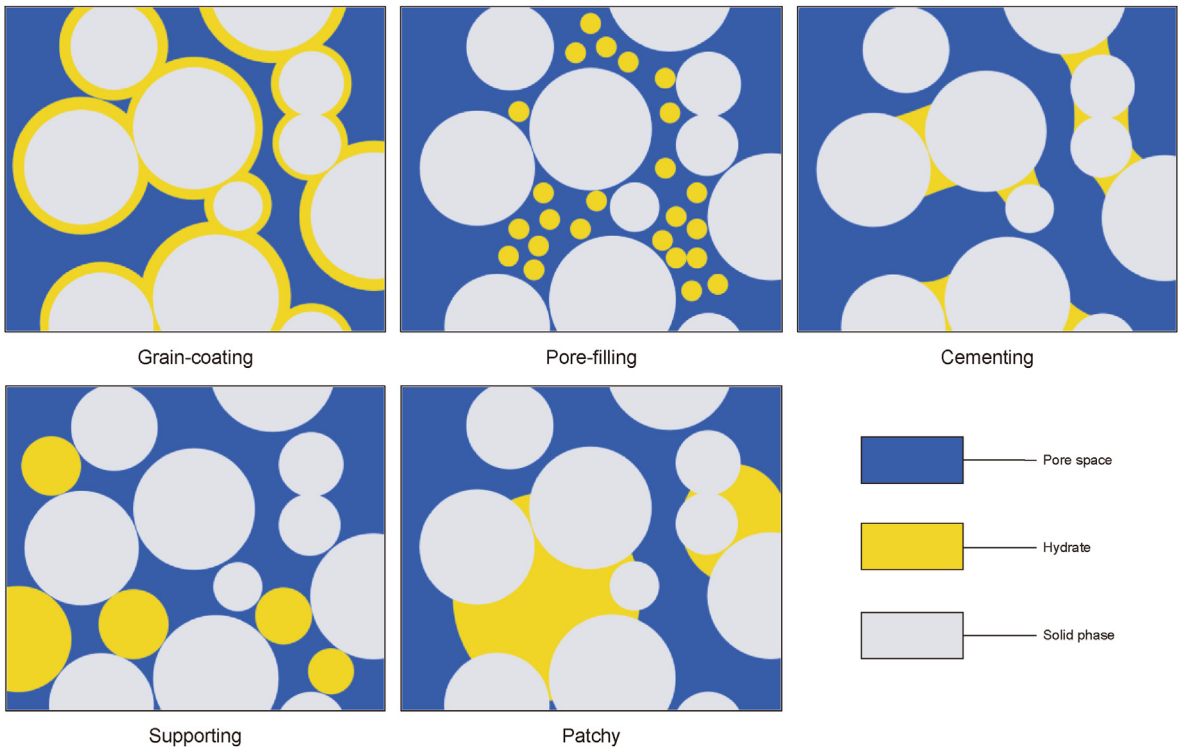

Fig. 8. Microscopic occurrence patterns of natural gas hydrates.

using the phase-field model. By matching the model with experimental data, it successfully determined the hydrate formation rate constant. Further numerical simulations revealed the formation and growth of hydrates in pores, providing a microscopic perspective on the permeability and hydrate distribution of hydrate-bearing sediments. Chen et al. (2018) simulated the distribution of hydrates by establishing computational HBS (hydrate-bearing sand) models. They added hydrate voxels to the original pore structure of sandstone and constructed a hydrate-bearing sedimentary rock model with three ideal pore distribution types: grain-attaching, coarse pore-filling, and dispersed pore-filling. First, a subset of the original pore structure was clipped, and a mask was created for the subset. A reinitialization algorithm (level set method) was used to index which voxels were particles and which were pores. Grain-attaching hydrates grow by converting pore voxels in contact with particles into hydrates. Ostwald ripening is achieved by converting pore voxels near existing hydrates into new hydrates. Coarse pore-filling hydrates start with a few isolated crystals in the pore and continue to grow by converting pore voxels adjacent to existing hydrates into new hydrate voxels. Dispersed pore-filling hydrates grow by randomly converting pore voxels (at least one voxel from the particle) into hydrate voxels. Lin et al. (2019) discussed the actual distribution of hydrates within pore spaces and the associated algorithms. By contrasting laboratory observations of hydrate distributions with numerical simulation results, they concluded that the mathematical morphology algorithm could simulate the formation and distribution of hydrates effectively. Applying this method to simulate hydrate distributions, a skeleton-type hydrate digital rock model can be created when the phase in contact with the rock is considered to be hydrate, whereas a fluid-type hydrate digital rock model is constructed when the phase predominantly occupying the pore space is treated as hydrate. Consequently, the 3D construction of hydrate digital rocks can be achieved by incorporating the mathematical morphology algorithm to introduce hydrates into the pore space. Wu et al. (2020) delineated the modeling process of hydrate-bearing digital rocks into two distinct steps: threshold segmentation and morphological operations, subsequently validating the algorithm's accuracy through comparisons with petrophysical simulations. Li et al. (2021) employed the same method to reconstruct sixteen 3D models, each with varying hydrate saturation levels and particle shapes. They subsequently investigated how these variables, in conjunction with varying hydrate saturations and particle shapes, influence other petrophysical properties based on these models.

Wu et al. (2023) proposed a hybrid simulation method that integrates CT technology, morphological algorithms, and the quartet structure generation set method (QSGSM) to construct GHBS models with specific hydrate distribution patterns and precise control over hydrate saturation, as illustrated in Fig. 9. The entire process comprises three stages: hydrate core selection, hydrate core growth, and hydrate formation. Initially, CT technology was used to create digital samples of HBS, followed by the application of morphological operations (MO) and QSGSM to simulate hydrates with tailored morphologies and saturation levels. Notably, QSGSM can produce objects with predefined dimensions and shapes, where porous media entities can include minerals, pores, organic compounds, or other microstructures. Following each iteration, the hydrate progressively expands from the core or central point into the surrounding voxels. Ultimately, 3D digital rock models featuring various hydrate patterns and saturation levels are generated. Dong et al. (2018b) were the first to employ the diffusion-limited aggregation (DLA) method to simulate hydrate growth, constructing models that represent cemented, dispersed, and adhesive hydrates across various saturation levels. The DLA method forms clusters by utilizing particles that move randomly and are generated from a selected point source. As the hydrate cluster expands, additional point sources are created. Upon

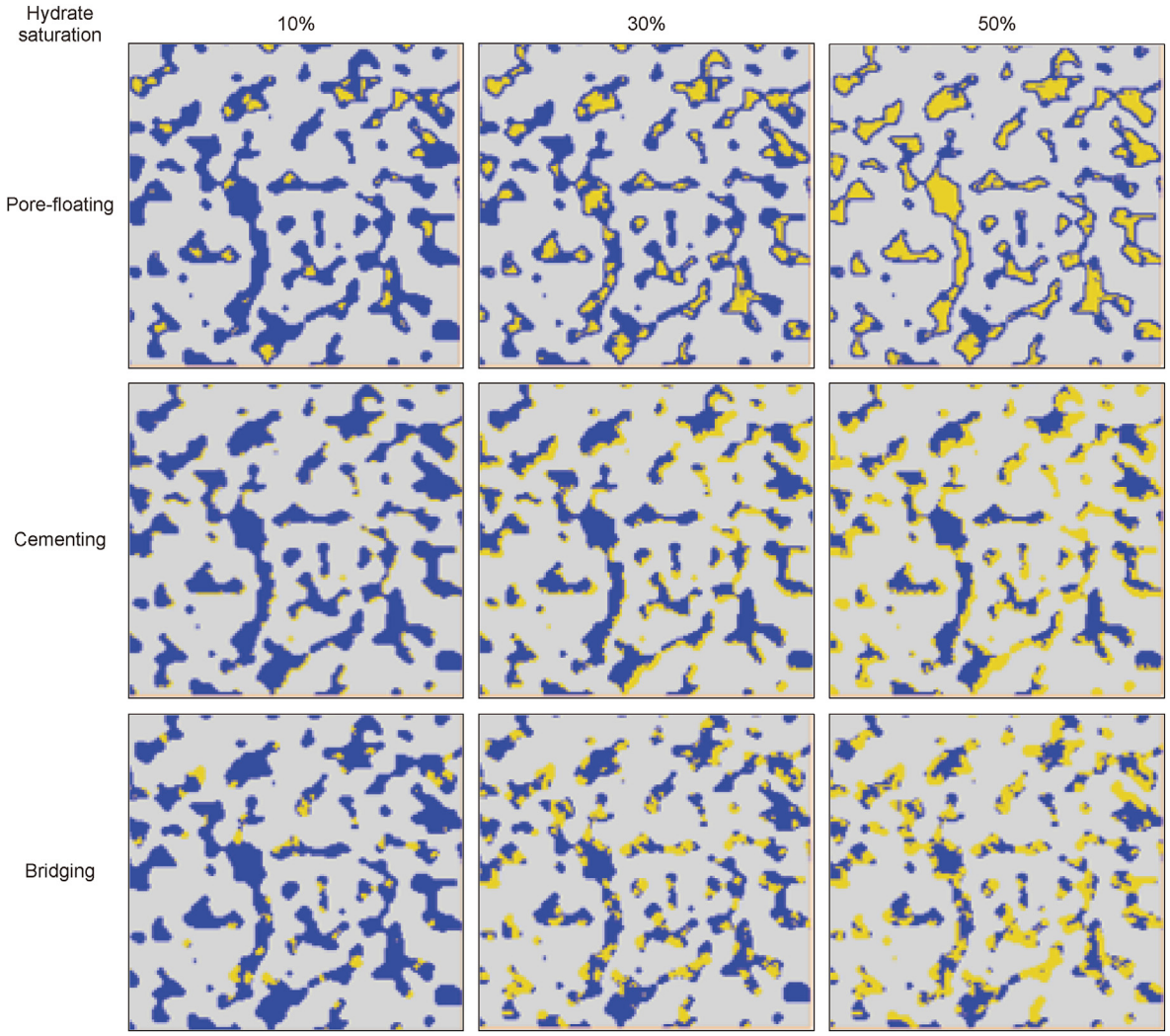

Fig. 9. Three hydrate occurrence patterns with different saturation levels in 2D slices. Gray represents the solid phase, blue represents the pore space, and yellow represents the hydrate (adapted with permission from Wu et al. (2023)).

reaching the hydrate cluster, the particles cease their random movement and remain in their final positions. Once the conditions for cluster growth reach a predefined threshold, the hydrate growth process ceases. Furthermore, in examining the effects of natural gas hydrate cementation models on rock properties, they employed an algorithm analogous to the process-based method to create 3D digital rocks exhibiting three distinct hydrate cementation models (Dong et al., 2018a). Hydrates uniformly coat the surfaces of rock grains, precipitate within pores, and accumulate in pore throats, enhancing the understanding of how hydrate cementation affects rock conductivity, stiffness, and pore interconnectivity. To a certain degree, the aforementioned methods can assist researchers in understanding the formation mechanisms of hydrates and their influence on rock properties. Given the intricate, variable, and unstable nature of hydrate formation in actual settings, these methodologies may require further refinement and expansion to meet a wider range of research requirements.

3. Rock petrophysical property simulations

3.1. Fluid flow simulation

3.1.1. Traditional CFD methods

Computational fluid dynamics (CFD) is a numerical analysis method utilized for simulating and analyzing fluid flow behavior. Traditional CFD techniques include FEM, FDM, and the finite volume method (FVM). These numerical methods enable the direct discretization and meshing of 2D or 3D models, solving the associated control equations, and obtaining the corresponding flow field distributions and permeability values.

Katagiri et al. (2017) developed permeability reduction models for cubic packs of cylinders and spheres containing grain-coating and pore-filling hydrates, as well as random sphere packs. These models were based on previous studies and used the discrete element method (DEM) to generate particle packs, which were then verified through pore-scale CFD simulations. The study revealed that the developed models closely matched the simulation outcomes and experimental data, providing petrophysical relevance to the proposed model parameters. Kossel et al. (2018) employed MRI to acquire a time-resolved, 3D map of natural gas hydrate saturation. These images were subsequently imported into the commercial finite element analysis software (COMSOL Multiphysics), where they applied five distinct permeability formulas to model the flow dynamics. This process elucidated the correlation between hydrate saturation levels and permeability. Zhang et al. (2022b) constructed a range of 2D geometric models including pore-filling and grain-coating types, and their combinations, based on samples of hydrate-bearing sediments and CT images. The team

applied the FEM to simulate the flow characteristics at the pore scale of these models. The simulations indicated that the hydrate distribution pattern, saturation level, and sediment particle size significantly influenced the permeability of hydrate-bearing sediments. Notably, the heterogeneous model developed in this study represents a pioneering approach for evaluating the permeability of hydrate-bearing sediments. In order to study the dynamic fluid flow characteristics of hydrate-bearing sediments, Xu et al. (2023) used CFD to simulate single-phase flow in a range of 2D idealized hydrate-bearing sediment models. The results indicated that the formation and growth of hydrates within the pores led to the evolution and transformation of the pore space structure. The primary cause of reduced GHBS permeability was the dominance of smaller pores and throats as hydrate saturation increased, which weakened the connectivity of the pore space and increased the distortion of fluid flow. Additionally, the growth of hydrates with different habits within the pores led to alterations in flow channels and their morphology, resulting in varied seepage behavior and permeability changes within the model. Yu et al. (2017) employed 3D unstructured mesh of regular cubic unit and CFD to calculate the dissociation rate of CH_4 hydrate in heterogeneous laboratory sediment samples. However, the study only simulated water flow and solid CH_4 hydrate, excluding the ice phase and gas phase.

CT technology can provide detailed microscopic structures of GHBS, which is beneficial for simulating fluid flow. When exploring the impact of hydrates on permeability at the pore scale, Pan et al. (2021) obtained the 3D pore structure of actual GHBS through micro-CT scanning. They employed the Finite-Difference Method Stokes Solver (FDMSS) to directly solve the single-phase flow equation on voxelized 3D pore structures, thereby obtaining the 3D velocity field and permeability. Their study revealed that the distribution of hydrates among pores significantly impacts permeability, with an uneven hydrate distribution leading to pronounced permeability anisotropy. Kou et al. (2021), on the other hand, used CT to capture the 3D pore structure of real CH_4 hydrate-bearing sediments. Subsequently, they performed CFD simulations using the commercial software Avizo XLab to visualize the 3D flow field within hydrate-containing porous media. Their findings indicated that the formation and growth of natural gas hydrates within pores altered the initial pore structure, resulting in pores that were no longer interconnected. Previously connected pores became blocked, the flow pathways changed, and the number of streamlines gradually diminished. The existence of these non-interconnected pores further complicates the analysis of the pore structure and the accuracy of permeability predictions. To investigate the evolution of hydrate behavior and its petrophysical impact in fractured-pore GHBS during phase transformation, Bian et al. (2022) created a 3D model of hydrate-saturated fractured sandstone using micro-CT images and employed CFD simulation to analyze the velocity, pressure, and permeability within the porous space. The results indicated that pressure changes triggered simultaneous hydrate synthesis and decomposition, establishing a dynamic equilibrium within the sediments. The occurrence of hydrates within fractured-porous media can be categorized into three distinct types: contiguous-sheet, clustered, and isolated hydrates. Notably, contiguous-sheet hydrates predominantly influenced the fluid flow characteristics of the fractured sediments. Li et al. (2023a) studied sediments from the Shenhu area in the South China Sea by employing a combination of particle flow code and CFD to simulate and study how the shape of mineral particles and the presence of pore-filling natural gas hydrates affect the anisotropic nature of permeability.

3.1.2. Pore network modeling

PNM can simplify the internal microstructure of porous media into a collection of geometries with specific shapes and sizes. By adjusting the parameters and arrangement of these geometries, it becomes possible to simulate the influence of different pore structures on permeability. This method provides an effective and convenient numerical simulation approach for studying permeability.

Liang et al. (2010) proposed the PNM to determine the effective permeability in hydrate-bearing porous media. They employed this technique to assess the effects of hydrate particle formation and growth patterns on permeability, and to examine the changes in permeability across various levels of hydrate saturation within porous media. The findings highlighted that the size and distribution of pores, which lead to displacement at hydrate equilibrium, are important factors in dictating the permeability of media containing hydrates. Following extensive validation against experimental results, PNM can be effectively used for studying the processes of hydrate formation and dissociation in porous media. Dai and Seol (2014) used random 2D pore networks to analyze the correlation between apparent water permeability and hydrate saturation, taking into account the hydrate growth at the pore scale and the heterogeneity at the meso scale. They reassessed existing capillary tube models and the Tokyo models, and introduced an enhanced Kozeny model that provided improved accuracy in estimating permeability. Jang and Santamarina (2011) utilized PNM to identify a minimal set of pore-scale parameters that are crucial for understanding natural gas recovery and water production, factors that hinge on initial hydrate saturation, the distribution of pore sizes, and P-T conditions. The PNM simulation outcomes can guide the choice of pertinent parameters for capillary pressure functions and relative permeability relations in finite element analysis. Mahabadi et al. (2019) investigated the influence of pore habits on permeability by assessing the impact of hydrate patch size using PNM. Hydrate saturation was determined by randomly distributing hydrates across ten identical pore networks. The simulations revealed that THF hydrates tend to form small clusters within the sediment, with an average patch size comprising approximately four pores. Mahabadi and Jang (2014) developed the PNM to simulate the dissociation of hydrates and the subsequent gas expansion within a dispersed hydrate system, with initial hydrate saturation levels ranging from 10% to 60%. The models, composed of pores interconnected by tubes, facilitated the distribution of hydrates. Subsequently, the relative permeability of both gas and water during the gas expansion process following hydrate dissociation was computed. The simulation outcomes guided the selection of fitting parameters, leading to the conclusion that the modified Stone equation can accurately predict the relative permeability of water and gas in sediments that produce gas from hydrates. Other researchers have also utilized geological drilling data for modeling purposes. For instance, Mohammadmoradi and Kantzas (2018) established a three-phase pore morphology model directly derived from the particle size distribution of samples from the Mallik site. This model was utilized to simulate the deformation of hydrates and to predict the fluid content, absolute permeability, and effective permeability in geological formations containing hydrates. It effectively replicated the laboratory findings regarding the spatial arrangement of fluids, the degree of tortuosity, and the permeability in sediments with hydrates. In contrast to other simulation frameworks that use PNM, this model provides a more straightforward method for examining various aspects of hydrate morphology, formation, and dissociation in porous media.

To more accurately simulate the permeability behavior of porous media, researchers widely utilize CT technology to construct PNM based on real image data. Wang et al. (2015a) were the first to integrate PNM with CT to accurately capture the actual structure of porous media containing hydrates. Using CT imaging,

they obtained data and simulated the flow of CH_4 and water, predicting changes in porosity, saturation, relative permeability, and capillary pressure. The results validated the feasibility and accuracy of the method. The team subsequently identified key parameters affecting the permeability of hydrate-bearing porous media using the same techniques, including hydrate particle size (Wang et al., 2016), wettability (Wang et al., 2015b), and interfacial tension (Wang et al., 2018b). Model calculations clarified the quantitative relationships between these parameters and permeability. Mahabadi et al. (2016) also employed this approach to extract micron-resolution CT images of Mallik site hydrate sediments and construct 3D pore networks. They implemented hydrates with varying saturations and morphologies into the network and further simulated processes including gas intrusion, hydrate dissociation, and gas-water permeation. These simulations helped determine appropriate parameters for characterizing the water retention curve and relative permeability of hydrate-bearing sediments. Ai et al. (2017) explored the permeability characteristics of irregular porous media containing CH_4 hydrates using sandstones with various morphologies, including quartz, dolomite, and feldspar. They used CT and PNM to conduct an in-depth analysis of the gas and water flow during the decomposition of hydrates and the subsequent effects on hydrate production. In a related study focusing on the influence of natural gas hydrate formation and decomposition on fluid flow within fine-grained quartz sand, Wang et al. (2018a) captured high-resolution CT images at different stages of the experiments. These images accurately revealed the internal pore structure, which was used to construct topologically characterized pore networks. Their analysis revealed that natural gas hydrates predominantly grew as particle cementation within the pore space, with hydrates filling or bridging pores during the intermediate stages. As hydrate saturation decreased during the decomposition process, there was an increase in water-phase permeability, a decrease in bound water saturation, and an increase in the gas-water two-phase flow area. While PNM accurately represents the macroscopic properties of porous media, simplifying the complex pore structure for mathematical modeling and computation can lead to the loss of detailed information regarding hydrate distribution and morphology.

3.1.3. Lattice Boltzmann method

LBM represents a novel CFD approach. Rooted in the Boltzmann equation from statistical physics, LBM simulates the distribution function of particle groups at discrete lattice sites to predict the behavior of macroscopic fluid properties. This method is especially adept at modeling complex porous media and microscale flows. In recent years, LBM has been extensively applied in research concerning fluid flow simulations within GHBS.

Kang et al. (2004) utilized LBM to simulate the crystallization process of hydrates in supersaturated solutions. This research represented an initial foray into computational investigations of the formation and decomposition of natural gas hydrates. Keehm and Yoon (2008) employed LBM to simulate fluids by generating GHBS numerical models with varying hydrate pore habits. They calculated permeability at different saturation levels. In another study, Kang et al. (2016) used LBM to explore the correlation between hydrate saturation levels and permeability throughout the hydrate formation process. They proposed a permeability model for hydrate-bearing sediments that accounts for capillary effects. This model separately considered the occurrence of grain-coating and pore-filling hydrates. The findings revealed that permeability diminished linearly with rising saturation during the grain-coating hydrate nucleation phase. Moreover, the permeability was higher than that of models that did not consider the capillary effect of hydrate nucleation. Additionally, a transition zone was observed between hydrate saturation levels of 30% and 40%. The decreasing trend of permeability shifted from the grain-coating model to the pore-filling model within this zone. The initial sediment density and grain size distribution had negligible effects on the change in permeability. Hou et al. (2018) conducted flow simulations in 2D homogeneous porous media using LBM. Fig. 10 displays the hydrate distribution and velocity field within the model. This figure illustrates that factors such as hydrate saturation, hydrate formation habit, and pore-centered hydrate distribution pattern all significantly influence the fluid flow characteristics of 2D porous media. Furthermore, a novel permeability model for hydrate-containing sediments was introduced and validated with experimental results. To understand how hydrate micromorphology and growth habits affect GHBS permeability, He et al. (2020) employed LBM to simulate microscopic-scale fluid flow in 2D porous media, accounting for the geometric variations and differing proportions of grain-coating and pore-filling hydrates. The results indicated that subtle geometric differences in hydrates could significantly alter permeability, even when the hydrate growth habit and saturation levels were constant. Ji et al. (2022) likewise applied this method to evaluate the relative permeability of water and gas within 2D porous media that contained hydrates. The research studied how hydrate saturation levels and growth habits affected the relative permeability of water and gas at the pore level. The findings indicated that an increase in hydrate saturation led to a reduction in the effective permeability for both water and gas. For pore-filling hydrates, the relative permeability for water and gas rose with an increase in hydrate saturation, but for grain-coating hydrates, it declined. The influence of solid wettability varied between wet-phase and non-wet-phase relative permeabilities. Additionally, microscale fluid distribution changes impacted the relative permeability of water and gas. Notably, the potential Jamin effect during hydrate gas production could significantly alter multiphase flow characteristics.

Some researchers have also combined CT technology with LBM to study the fluid flow characteristics of GHBS. Chen et al. (2018) established a functional connection between the gas relative permeability at the microscopic level and the saturation of hydrates in real hydrate-bearing sandstones by combining micro-CT imaging and proposed a modified Corey model to better represent the data. Sun et al. (2021) also combined CT with LBM to study how particle size distribution and initial brine saturation influence permeability alterations in sediments during the dissociation of hydrates. LBM can simulate multiple coupled petrophysical and chemical processes under non-isothermal conditions in porous media, and it accounts for the evolution of the pore structure, making it well-suited for capturing intricate interactions within porous environments. Zhang et al. (2019b) developed a pore-scale model based on the LBM to address the reaction transport and non-isothermal multi-petrophysical and chemical processes occurring in porous media. This model provided a more precise depiction of the phase transition and evolution of pore structures during the dissociation of CH_4 hydrates, considering various hydrate pore habits. Additionally, they examined the impact of the temperature field, the inlet temperature, and inlet pressure on the dissociation of hydrates. The findings indicated that numerically simulating the decomposition of CH_4 hydrates at the pore-scale helps to deepen the understanding of the permeability-saturation relationship in continuous media models.

3.1.4. Molecular dynamics

Molecular dynamics (MD) is a computational simulation method that solves classical mechanics equations to simulate the interactions and movements of atoms and molecules over a specific period. This method has been proven to be an effective tool for studying the microscopic mechanisms of hydrates and provides not

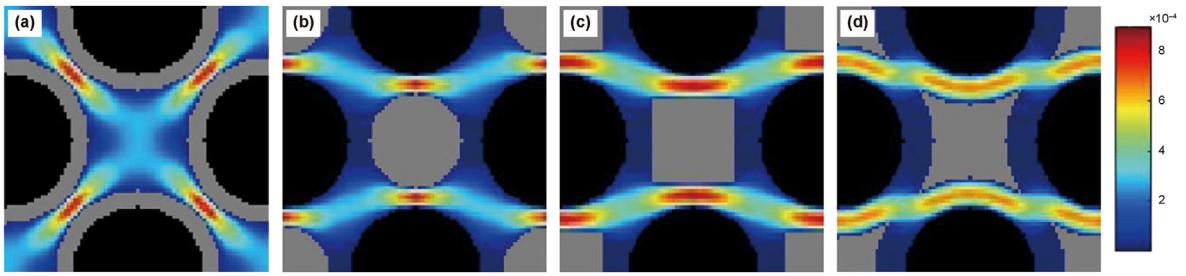

Fig. 10. Velocity field obtained from LBM calculations (adapted with permission from Hou et al. (2018)). The black represents mineral particles, the gray represents hydrates, and the colored fluid represents the velocity field derived from LBM.

only insights into the thermophysical properties of gas hydrate systems but also important information about hydrate equilibrium, thermodynamics, and structural properties (Li et al., 2023c; English and Tse, 2010; Veesam et al., 2019; English et al., 2009; Chen et al., 2022; Miyoshi et al., 2007). MD simulations possess a broad spectrum of applications, particularly in modeling the formation and dissociation of hydrates at the molecular scale (Das et al., 2022; Zhang et al., 2022d).

Yasuoka and Murakoshi (2000) used MD simulations to study the dissociation process of CH_4 hydrates. They constructed a simulation system with water and CH_4 molecules and simulated the decomposition of the hydrate structure and molecular behavior, revealing the structural changes occurring during the dissociation process. Moon et al. (2003) used MD simulations to study the mechanisms of CH_4 hydrate formation. The results revealed that under moderate subcooling conditions, water molecules rapidly formed ordered structures characteristic of hydrates, comparable in size to the predicted critical nucleus, providing significant insights into the formation of hydrates. Fang et al. (2019) focused on the dissociation dynamics of natural gas hydrates in sandstone reservoirs. By simulating the dissociation of hydrates under different initial temperature conditions, their study elucidated the relationship between temperature, hydrate structure, and the migration of CH_4 molecules. As depicted in Fig. 11, it demonstrates the temporal variation of the hydrate structure using MD simulations and how CH_4 molecules are liberated from the hydrate structure and accumulate to form nanobubbles on the silica surface. Phan et al. (2023) used non-equilibrium MD simulations to study the microscopic mechanism of CH_4 hydrate growth in a three-phase system. They specifically concentrated on the effects of additives, such as polyvinyl caprolactam oligomer and sodium dodecyl sulfate (SDS), on the growth rate of hydrates and elucidated how these additives modulate the growth kinetics of hydrates by altering the solubility of CH_4 in the aqueous phase. In their research on CO_2 hydrates, Sarupria and Debenedetti (2011) employed MD to investigate the dissociation behavior of CO_2 hydrates under varying occupancy rates and temperature conditions. By simulating systems in which hydrates were in contact with liquid water, the researchers quantified both the rate at which CO_2 was released from the hydrate structure into liquid water and the velocity of the hydrate-water interface movement. They concluded that the rate of hydrate dissociation was influenced not only by the overall occupancy but also closely correlated with the cage-specific occupancy. Using MD simulations, Zhang et al. (2019c) examined the formation process of CO_2 hydrates by constructing models with varied initial conditions to observe the dynamics of water and CO_2 molecules. This research delved into the mechanistic basis of hydrate formation and comprehensively evaluated the effects of variables such as temperature and CO_2 concentration on hydrate formation. The results demonstrated that system temperature and CO_2 molecule concentration significantly influence the structures and diffusion dynamics of water molecules. Lower temperatures and higher CO_2 concentrations were found to favor the formation of hydrates.

The integration of experimental data with MD simulation results can significantly enhance our understanding of the growth and dissolution processes of hydrates while validating the accuracy of the simulations. Choudhary et al. (2017) combined MD simulations and experimental research to investigate the effects of methanol and sodium chloride, two additives, on the growth of CH_4 hydrates. Their findings indicated that these additives function as promoters of hydrate growth at low concentrations. Cai et al. (2023) also combined MD simulations with experimental verification to study the effects of THF and SDS on the growth of CO_2 hydrates under different temperature and concentration conditions. The

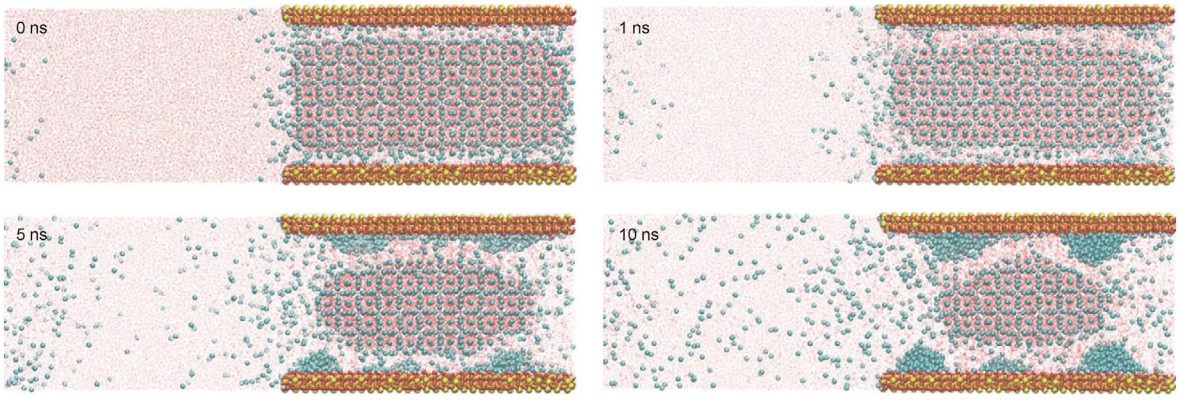

Fig. 11. Dissociation process of hydrate cluster in the nanopore (reprinted with permission from Fang et al. (2019)). The image uses different colors to distinguish different elements, with silicon (Si) represented in yellow, oxygen (O) in red, hydrogen (H) in white, and carbon (C) in cyan.

study revealed that the synergistic effect of THF and SDS significantly promoted hydrate growth at lower temperatures; however, at elevated temperatures, SDS molecules aggregated due to the presence of THF, leading to reduced THF and CO_2 concentrations at the hydrate-liquid interface, thereby adversely affecting hydrate growth. The experimental results also strongly supported these simulation findings.

It is noteworthy that MD simulations have reached a relatively mature stage in studying the nucleation, growth, and dissolution processes of gas hydrates, with significant progress achieved. Many scholars have provided detailed reviews on this topic (English and MacElroy, 2015; Kondori et al., 2017; Das et al., 2022; Zhang et al., 2022d). MD simulations are expected to make further breakthroughs in multi-scale modeling and enhance simulation accuracy, which will provide more powerful tools for a deeper understanding of the micro-mechanisms of gas hydrates (English and MacElroy, 2015).

3.2. Electrical property simulation

The electrical properties of hydrates, such as resistivity and dielectric constant, are considered reliable indicators for assessing the properties of hydrate matrices. The saturation and distribution of natural gas hydrates in sediments greatly influence the electrical properties. Investigating the electrical properties of GHBS facilitates the identification of hydrate reservoirs and the assessment of natural gas reserves. With the rapid advancement of digital rock technology, significant progress has been made in the simulation and study of electrical properties in GHBS. This technology integrates high-precision imaging and numerical simulation methods, enhancing our capability to comprehensively understand and predict the electrical behavior of GHBS. Fig. 12 illustrates a flowchart of the electrical simulation process, clearly presenting the complete procedure from geological sample acquisition to simulation result analysis. In the course of electrical simulations, the integration of 3D visualization and precise parameter computation facilitates accurate analyses of the electrical properties of GHBS. Researchers have developed various techniques to investigate the electrical characteristics of rocks, including lattice gas automaton methods, FEM, and FDM. Among these, FEM is the predominant method employed for investigating the electrical properties of natural gas hydrates.

Dong et al. (2018b) created a porous digital rock model, including hydrates, based on CT images from hydrate reservoir rock samples in China's western frozen soil belt and investigated how hydrate distribution, saturation, and salinity impact electrical properties using FEM. The study found that for the three types of hydrate digital rocks at equal saturation, resistivity decreased as formation salinity increased. Among these, the resistivity was highest for adhesive hydrate digital rocks, lower for cemented hydrate digital rocks, and the lowest for scattered hydrate digital rocks. Differences in resistivity among the various hydrate digital rock types increased as saturation levels increased, becoming significant when the saturation level surpassed 55%. Additionally, they generated 3D digital rocks with varying hydrate cementation models using process-based methods and growth algorithms. They then studied the impact of these models on rock electrical properties via FEM. With increasing hydrate saturation, they found that electrical parameters increased across all cementation models. Additionally, under identical hydrate saturation conditions, the resistivity of hydrates in pore throats was greater than that of hydrates precipitating within the pores (Dong et al., 2018a). Based on prior work, Dong (2020) developed two types of digital rock models featuring hydrates: pore-type and fracture-type models. Using this foundation, FEM was used to explore how different hydrate distributions and cementation patterns affect rock electrical properties, analyze the changes in resistivity with hydrate saturation, and establish a model for ideal hydrate saturation calculations. Xing et al. (2021) aimed to clarify the intricate conductive properties of porous media containing natural gas hydrates and establish the relationship between hydrate saturation and complex conductivity attributes. They used COMSOL Multiphysics finite element software to simulate complex conductivity responses under different conditions. The results indicated that variations in natural gas hydrate content significantly impacted sediment resistivity within a defined frequency range, and a power-law relationship was established that correlated resistivity parameters with hydrate saturation in log-log space. Furthermore, the relationship between hydrate saturation and composite conductivity was influenced by the salinity of pore water. Notably, when the pore water conductivity exceeded 1.0 S/m, a stable power-law correlation between hydrate saturation and orthogonal conductivity emerged, offering a novel theoretical foundation for assessing hydrate saturation. The study further investigated the influence of hydrate micro-distribution patterns on resistivity characteristics, yielding significant insights into understanding the resistivity features of natural gas hydrate sediments. To explore the electrical characteristics of fractured hydrate-bearing reservoirs, Yang et al. (2021) used CT technology to capture the microstructure of rock samples and constructed a corresponding digital rock model. They applied the diffusion-limited aggregation (DLA) model to represent hydrate distribution. Utilizing finite element analysis, they thoroughly examined how fractures and hydrates influence rock electrical properties, focusing on the relationship between resistivity index and water saturation. The findings indicated that the electrical properties of rocks could not be accurately described by the traditional Archie's equation. Specifically, the resistivity index of fractured gas hydrate reservoirs showed a nonlinear relationship with water saturation, and this relationship had different characteristics for different types of gas hydrate pores. Wu et al. (2023) created 75 digital rock models with specified hydrate saturation levels using a novel method that incorporated three occurrence patterns: pore-floating, cementation, and bridging. Using FEM, they investigated how hydrate distribution and saturation impact conductivity and validated the models' reliability and accuracy against laboratory measurements. Lan et al. (2023) quantitatively analyzed the relationship between hydrate morphology and resistivity by examining different hydrate skeleton particle arrangements, occurrence patterns, and distribution morphologies in a 2D geometric model. They applied FEM to solve the electric field equation for porous media, assuming a constant flow field, and derived the resistivity value for media containing hydrates. This study identified three stages in the change in resistivity with hydrate saturation: minimal impact, gradual change, and sharp increase. At low hydrate saturations, the resistivity of the pressure model remained relatively high compared to that of the particle cementation and pore-filling models. Furthermore, they discovered that the throat size was the primary factor influencing resistivity.

Some researchers have also used other numerical methods, such as the FVM and the Kirchhoff node method, to study the electrical properties of hydrates. Wu et al. (2020) created 14 models featuring varying hydrate saturation levels and occurrence states, such as cementing and pore-filling. By combining PNM with the FVM, they studied how particle shape and hydrate saturation affect the conductivity of hydrate-bearing sediments, obtaining numerical results that closely matched published data. Tian et al. (2023) utilized commercial Avizo software for numerical simulation to study the relationship between the normalized permeability and the resistivity index in GHBS. Avizo software calculates electrical properties using a volume averaging method based on Ohm's law, determining the macroscopic equivalent resistivity by weighting

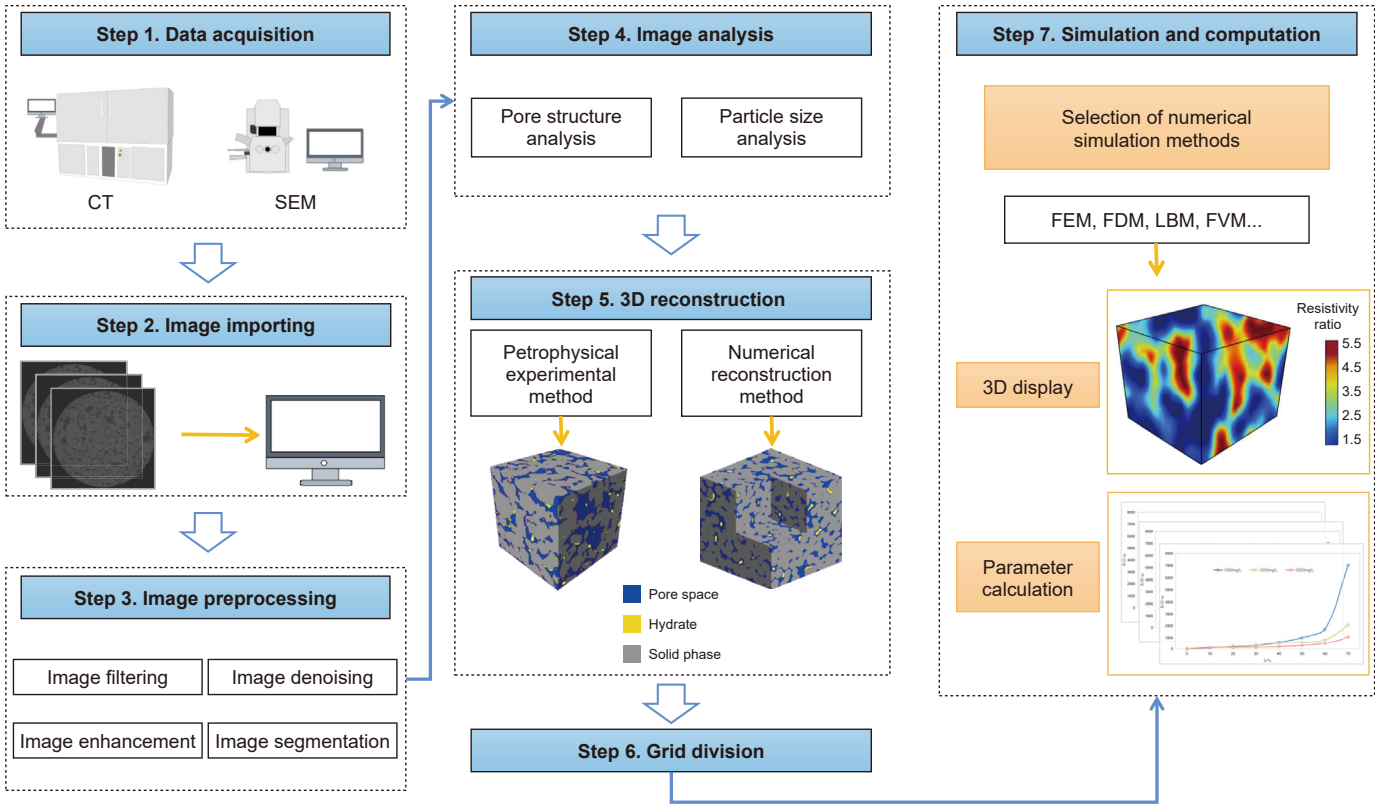

Fig. 12. The flowchart of the electrical simulation process.

the electrical properties of different phases in the multiphase medium. The results indicate a negative power-law relationship between the resistivity index and normalized permeability, with the power-law index influenced by the fractal dimension of tortuosity. The accuracy of the model was validated through comparisons with laboratory and well log data, providing a novel theoretical foundation and computational method for the electrical prediction of natural gas hydrate reservoirs. Zhao et al. (2021) used a pore network to represent the pore space in natural gas hydrate reservoirs and applied the Kirchhoff node method to calculate current parameters within the model. Numerical simulations were conducted to examine how natural gas hydrate saturation affects the resistivity of digital rocks under varying porosities, formation water salinities, and clay mineral contents. The study revealed that resistivity increased exponentially as hydrate saturation increased, and the resistivity of the natural gas hydrate digital rock model decreased linearly with increasing formation water conductivity. An increase in clay mineral content resulted in a negative exponential trend in rock resistivity. The findings imply that at low porosities and clay mineral contents, natural gas hydrate saturation significantly affects the resistivity of digital rocks.

3.3. Elastic property simulation

Digital rock technology plays an important role in analyzing the elastic characteristics of hydrates. This technology uses computer simulation and numerical methods to simulate the microstructure and properties of hydrates by establishing mathematical models of rocks and conducts quantitative research on the influence of reservoir parameters on the elastic characteristics of GHBS.

In the analysis of the elastic properties of hydrates through digital rock technology, FEM is routinely employed for numerical calculations. The principle of FEM for calculating elasticity is based on dividing the continuous media into discrete small units, known as finite elements. Within each finite element, an appropriate mathematical model is established, and mechanical principles and boundary conditions are then applied to determine the stress, strain, and displacement parameters of the system (Garboczi, 1998). Lin et al. (2019) developed two different hydrate digital rock models based on hydrate petrophysical models. Using FEM, they calculated the elastic properties of the rock models and confirmed their consistency with the petrophysical models through a combination of numerical simulations and theoretical analysis. Additionally, they observed that the distribution of hydrates in the area resembled the skeletal model pattern. Dong et al. (2018a) used FEM to determine stress distribution and effective elastic parameters of 3D digital rocks. With increasing hydrate saturation, elastic parameters also increased. Under equivalent hydrate saturation conditions, the pore-throat type exhibited larger elastic parameters compared to the pore-precipitation type. This difference is attributed to the increased contact area between rock particles caused by hydrates in the pore throats, which facilitates enhanced compression. Li et al. (2022) used high-resolution 3D images obtained from synchrotron X-ray CT to construct a series of sediment models with varying gas hydrate saturations. Using FEM, they quantitatively simulated the elastic responses of these models under different gas hydrate morphologies, tracking changes in the elastic modulus and wave velocity. The study found that at low gas hydrate saturations, hydrates predominantly form around the gas phase, leading to a significant increase in bulk modulus and compressional wave velocity. In contrast, the shear modulus and shear wave velocity are relatively less affected due to the water films that insulate the gas hydrates from the solid particles. As gas hydrate saturation increases, the changing morphology of the gas hydrates significantly

enhances the elastic characteristics of the sediment. Wu et al. (2023) utilized finite element analysis to study how the distribution pattern and saturation level of hydrates influence the elastic modulus. The study revealed that the presence of bridging hydrates leads to the most rapid increase in both the bulk modulus and shear modulus of sediments. Tian et al. (2024) conducted a study in which two types of digital rock models were obtained using the process-based method and CT. Based on these models, three common hydrate morphologies were simulated using the random simulation method. The corresponding elastic modulus was then numerically simulated with the assistance of finite element software Elas3D. The findings illustrated that the efficacy of the uncemented sand model is contingent upon the sample's original porosity, whereas the predictive capability of the cemented sand model regarding shear modulus is limited. To investigate the effects of different hydrate distribution patterns on petrophysical properties of fractured reservoirs, Liu et al. (2024) constructed digital rock models with regular fractures and simulated fractured hydrate-bearing digital rocks with multiple hydrate distributions by inserting different forms of hydrates. They utilized FEM to calculate anisotropic elastic characteristics. The findings showed that higher levels of hydrate saturation correspond to greater anisotropy in elastic wave velocity in fractured reservoirs, particularly demonstrating a significant impact from bridging hydrate distribution on wave velocity. This suggests that bridging hydrates act as a structural matrix in fractures, significantly improving elastic stiffness in the vertical direction. This discovery is crucial for further understanding how hydrate distribution impacts seismic wave propagation behavior in fractured reservoirs and provides a new theoretical basis for applying seismic exploration technology to evaluate hydrate resources.

4. Conclusions and future prospects

Digital rock technology is a key tool for quantitatively revealing the microscopic characteristics of rock pore structure and exploring the petrophysical properties of GHBS. We summarize the main methods used to construct digital rock models of gas hydrates and extensively discuss the advantages and disadvantages of these methods. Additionally, we analyze the methods for simulating petrophysical properties such as electrical, elastic, and fluid flow characteristics based on digital rocks. In this section, we provide a summary of the applications of digital rock technology in studying the petrophysical properties of GHBS, along with current challenges and prospects.

(1) The X-ray CT scanning method is the primary digital rock reconstruction method used to study GHBS. It provides the pore structure and hydrate distribution of GHBS through non-destructive tomography and computer processing. Although the application of CT technology in the research of natural gas hydrates has advanced significantly, it continues to face challenges related to image resolution and component identification. Improving resolution requires the use of high-precision instruments, but the high cost and technical complexity restrict its widespread application. To address the issue of component identification, researchers enhance contrast by adding soluble salts or using hydrates with different guest molecules. With advancements in artificial intelligence, utilizing deep learning to identify different component types and improve image resolution may be an important development approach.

(2) MRI serves as an important visualization tool for monitoring the formation and decomposition of gas hydrates, providing information on hydrate saturation, component identification, and pore distribution. However, its limited resolution cannot fully reveal the microstructure of gas hydrates. SEM offers extremely high resolution and can obtain structural features at the nanoscale; nevertheless, due to the limited observation area, it is difficult to study the overall structure of hydrate samples. Despite these challenges, the application of these technologies in gas hydrate research demonstrates considerable potential, serving as critical tools for the comprehension of the internal structure and properties of gas hydrates. Future research directions will prominently involve the utilization of deep learning methods to integrate information derived from images of diverse sources and scales, thereby facilitating the construction of 3D digital rock models.

(3) The process-based method is the main numerical reconstruction approach utilized in studying GHBS. Widely favored for its cost-effectiveness and flexibility, this method simulates the sediment formation process. However, it is applicable to GHBS research with relatively simple sediment particles. Given the complexity and instability inherent in the actual formation process, existing simulation methods still necessitate further refinement and expansion.

(4) For the simulation of the petrophysical properties of GHBS, the study of fluid flow characteristics is important for both reservoir evaluation and development, thus attracting considerable research attention. Traditional simulation methods offer high theoretical accuracy but face challenges such as high computational costs and complex mesh preprocessing. The PNM method demonstrates strong adaptability and practicality in porous media fluid flow characterization, but it requires careful selection of appropriate parameters and reasonable simplification of the model to balance accuracy and computational efficiency. In contrast, LBM has unique advantages in handling complex interactions in porous media, featuring simple programming and high accuracy. However, there is a gap between the ideal porous media model and the actual situation, and the phase changes of hydrates during the flow process also need to be considered in future research. MD simulations offer distinctive advantages in elucidating the growth and dissociation mechanisms of natural gas hydrates at the microscopic level, and future developments aim to achieve more profound understanding and accurate predictions through multi-scale modeling and enhanced simulation accuracy. Although there is relatively little research on electrical and elastic simulations, understanding their importance for the accuracy of GHBS geophysical exploration interpretation is also crucial. Specifically, the analysis of the electrical and elastic properties of GHBS and the development of geophysical exploration interpretation models are key objectives for analyzing the petrophysical properties from a microscopic perspective. It is evident that imaging techniques can capture the relative positional relationships between hydrates and mineral particles, but they are insufficient in providing information on the coupling strength between them, which is a critical factor in determining the stiffness and velocity of GHBS. It is essential to conduct in-depth research on defining the elastic parameters of hydrates under varying occurrence patterns and saturation levels, incorporating them as dynamic variables in simulating the elastic properties of GHBS. Furthermore, it is essential to recognize that different models of hydrate occurrence affect various physical properties of the reservoir, such as its elastic, electrical, and permeability characteristics. Therefore, the choice of simulation methods for petrophysical properties may vary accordingly.

Nevertheless, existing comparative studies concerning numerical simulation methods for different hydrate occurrence patterns are still scarce, highlighting a need for further exploration in this field.

(5) With the continuous advancement of high-precision instruments, the construction of digital rock models is no longer limited to a single technical approach. It can be integrated with a variety of instruments to thoroughly investigate the complex properties and formation mechanisms of hydrates at the nanoscale to the macroscale, taking into account the characteristics of natural gas hydrates in different regions. Simultaneously, the 3D digital rock models with multi-scale, multi-component, and high-resolution can be established based on a wider range of core analysis data, such as well log-based lithology and mineral composition analysis data, mercury injection capillary pressure data, and T_1–T_2 2D NMR analysis data, in order to more accurately depict the intricate reservoirs containing natural gas hydrates.

(6) In future research on hydrates, the focus should be on integrating multiple technologies to achieve comprehensive and accurate detection of the petrophysical properties of GHBS. This involves combining geophysical exploration technology with digital rock technology to conduct more thorough petrophysical property analyses. Geophysical exploration techniques such as well logging, seismic, electrical, and electromagnetic methods can provide extensive information about the macroscopic distribution of hydrates, while digital rock technology can offer detailed insights into the internal structure of sediments. This interdisciplinary research approach will provide a new perspective for understanding the relationship between microstructure and macroscopic behavior in natural gas hydrate systems. By incorporating advanced imaging techniques, computational simulations, and data analysis tools, researchers can comprehensively capture the complexity of GHBS, thereby optimizing resource assessment and improving exploitation efficiency.

CRediT authorship contribution statement

Yang-Chen Fan: Writing – original draft, Methodology, Investigation. **Wei-Chao Yan:** Writing – review & editing, Supervision, Project administration, Funding acquisition. **Hui-Lin Xing:** Writing – review & editing, Funding acquisition. **Xiu-Juan Wang:** Writing – review & editing, Funding acquisition. **Huai-Min Dong:** Methodology, Funding acquisition. **Xi-Mei Jiang:** Writing – original draft. **Ji-Lin Zhou:** Methodology.

Declaration of competing interest

The authors declare that they have no known competing financial interests or personal relationships that could have appeared to influence the work reported in this paper.

Acknowledgements

This research work was funded by the National Key R&D Program of China (2023YEE0119900), National Natural Science Foundation of China (Nos. 92058211, 42204105 and 42121005), Fundamental Research Funds for the Central Universities (No. 862201013140), 111 project (No. B20048), the International (Regional) Cooperation and Exchange Programs (No. 12411530092), the Young Talent Fund of Association for Science and Technology in Shaanxi (No. 20230703) and Technology Innovation Leading Program of Shaanxi (No.2024 ZC–YYDP–27).

References

Abegg, F., Bohrmann, G., Freitag, J., Kuhs, W., 2007. Fabric of gas hydrate in sediments from Hydrate Ridge—results from ODP Leg 204 samples. Geo Mar. Lett. 27, 269–277. https://doi.org/10.1007/s00367-007-0080-4.

Ai, L., Zhao, J., Wang, J., Song, Y., 2017. Analyzing permeability of the irregular porous media containing methane hydrate using pore network model combined with CT. Energy Proc. 105, 4802–4807. https://doi.org/10.1016/j.egypro.2017.03.950.

Alshibli, K., Jarrar, Z., 2021. Four-dimensional dynamic synchrotron microcomputed tomography imaging of gas-water interface at high pressure and low temperature. Geotech. Test. J. 44, 20190332. https://doi.org/10.1520/GTJ20190332.

Bagherzadeh, S., Moudrakovski, I., Ripmeester, J., Englezos, P., 2011. Magnetic resonance imaging of gas hydrate formation in a bed of silica sand particles. Energy Fuels 25 (7), 3083–3092. https://doi.org/10.1021/ef200399a.

Bakke, S., Øren, P., 1997. 3-D Pore-scale modelling of sandstones and flow simulations in the pore networks. SPE J. 2 (2), 136–149. https://doi.org/10.2118/35479-PA.

Baldwin, B., Moradi-Araghi, A., Stevens, J., 2003. Monitoring hydrate formation and dissociation in sandstone and bulk with magnetic resonance imaging. Magn. Reson. Imaging 21 (9), 1061–1069. https://doi.org/10.1016/j.mri.2003.05.001.

Bian, H., Qin, X., Luo, W., Ma, C., Zhu, J., Lu, C., Zhou, Y., 2022. Evolution of hydrate habit and formation properties evolution during hydrate phase transition in fractured-porous medium. Fuel 324, 124436. https://doi.org/10.1016/j.fuel.2022.124436.

Blunt, M., Bijeljic, B., Dong, H., Gharbi, O., Iglauer, S., Mostaghimi, P., Paluszny, A., Pentland, C., 2013. Pore-scale imaging and modelling. Adv. Water Resour. 51, 197–216. https://doi.org/10.1016/j.advwatres.2012.03.003.

Bohrmann, G., Kuhs, W., Klapp, S., Techmer, K., Klein, H., Murshed, M., Abegg, F., 2007. Appearance and preservation of natural gas hydrate from Hydrate Ridge sampled during ODP Leg 204 drilling. Mar. Geol. 244 (1–4), 1–14. https://doi.org/10.1016/j.margeo.2007.05.003.

Cai, X., Worley, J., Phan, A., Salvalaglio, M., Koh, C., Striolo, A., 2023. Understanding the effect of moderate concentration SDS on CO_2 hydrates growth in the presence of THF. J. Colloid Interface Sci. 658, 1–11. https://doi.org/10.1016/j.jcis.2023.11.136.

Chaouachi, M., Falenty, A., Sell, K., Enzmann, F., Kersten, M., Haberthür, D., Kuhs, W., 2015. Microstructural evolution of gas hydrates in sedimentary matrices observed with synchrotron X-ray computed tomographic microscopy. Geochem. Geophys. Geosy. 16 (6), 1711–1722. https://doi.org/10.1002/2015GC005811.

Chen, Y., Takeya, S., Sum, A., 2022. A clathrate hydrate structure hidden in plain sight. J. Phys. Chem. Lett. 13 (37), 8673–8676. https://doi.org/10.1021/acs.jpclett.2c02170.

Chen, Q., Liu, C., Ye, Y., 2012. Differential scanning calorimetry research of hydrates phase equilibrium in porous media. Adv. Mater. Res. 512–515, 2122–2126. https://doi.org/10.4028/www.scientific.net/amr.512-515.2122.

Chen, X., Espinoza, D., 2018. Ostwald ripening changes the pore habit and spatial variability of clathrate hydrate. Fuel 214, 614–622. https://doi.org/10.1016/j.fuel.2017.11.065.

Chen, X., Verma, R., Espinoza, D., Prodanović, M., 2018. Pore-scale determination of gas relative permeability in hydrate-bearing sediments using X-ray computed micro-tomography and lattice Boltzmann method. Water Resour. Res. 54 (1), 600–608. https://doi.org/10.1002/2017WR021851.

Cheng, C., Zhao, J., Song, Y., Zhu, Z., Liu, W., Zhang, Y., Yang, M., Yu, X., 2013. In-situ observation for formation and dissociation of carbon dioxide hydrate in porous media by magnetic resonance imaging. Sci. China Earth Sci. 56, 611–617. https://doi.org/10.1007/s11430-012-4570-5.

Chi, P., Sun, J., Yan, W., Cui, L., 2024. From digital rock to digital wellbore: multiscale reconstruction and simulation. Adv. Geo. Energy. Res. 13 (1), 1–6. https://doi.org/10.46690/ager.2024.07.01.

Chibura, P., Zhang, W., Luo, A., Wang, J., 2022. A review on gas hydrate production feasibility for permafrost and marine hydrates. J. Nat. Gas Sci. Eng. 100, 104441. https://doi.org/10.1016/j.jngse.2022.104441.

Chong, Z., Yang, S., Babu, P., Linga, P., Li, X., 2016. Review of natural gas hydrates as an energy resource: prospects and challenges. Appl. Energy 162, 1633–1652. https://doi.org/10.1016/j.apenergy.2014.12.061.

Choudhary, N., Kushwaha, O., Bhattacharjee, G., Chakrabarty, S., Kumar, R., 2017. Molecular dynamics simulation and experimental study on the growth of methane hydrate in presence of methanol and sodium chloride. Energy Proc. 105, 5026–5033. https://doi.org/10.1016/j.egypro.2017.03.1008.

Collett, T., Bahk, J., Baker, R., Boswell, R., Divins, D., Frye, M., Goldberg, D., Husebø, J., Koh, C., Malone, M., Morell, M., Myers, G., Shipp, C., Torres, M., 2014. Methane hydrates in nature current knowledge and challenges. J. Chem. Eng. Data 60 (2), 319–329. https://doi.org/10.1021/je500604h.

Dai, J., Xu, H., Snyder, F., Dutta, N., 2004. Detection and estimation of gas hydrates using rock physics and seismic inversion: examples from the northern deepwater Gulf of Mexico. Lead. Edge 23 (1), 60–66. https://doi.org/10.1190/1.1645456.

Dai, S., Santamarina, J., Waite, W., Kneafsey, T., 2012. Hydrate morphology: physical properties of sands with patchy hydrate saturation. J. Geophys. Res. 117, B11205. https://doi.org/10.1029/2012JB009667.

Dai, S., Seol, Y., 2014. Water permeability in hydrate-bearing sediments: a pore-scale study. Geophys. Res. Lett. 41 (12), 4176–4184. https://doi.org/10.1002/2014GL060535.

Das, S., Tadepalli, K., Roy, S., Kumar, R., 2022. A review of clathrate hydrate nucleation, growth and decomposition studied using molecular dynamics simulation. J. Mol. Liq. 348, 118025. https://doi.org/10.1016/j.molliq.2021.118025.
Denning, S., Majid, A., Koh, C., 2022. Stability and growth of methane hydrates in confined media for carbon sequestration. J. Phys. Chem. C 126 (28), 11800–11809. https://doi.org/10.1021/acs.jpcc.2c02936.
Dong, H., Sun, J., Arif, M., Liu, X., Golsanami, N., Yan, W., Cui, L., Zhang, Y., 2022b. A method for well logging identification and evaluation of low-resistivity gas hydrate layers. Pure Appl. Geophys. 179 (9), 3357–3376. https://doi.org/10.1007/s00024-022-03120-x.
Dong, H., Sun, J., Arif, M., Zhang, Y., Yan, W., Iglauer, S., Golsanami, N., 2022a. Digital rock-based investigation of conductivity mechanism in low-resistivity gas hydrate reservoirs: insights from the Muli area's gas hydrates. J. Petrol. Sci. Eng. 218, 110988. https://doi.org/10.1016/j.petrol.2022.110988.
Dong, H., 2020. Numerical Simulation on the Conductivity Mechanism of Low-Resistivity Gas Hydrate Reservoir in Muli Area. Ph.D. Thesis, China University of Petroleum (East China), Qingdao, China, pp. 36–84 (in Chinese).
Dong, H., Sun, J., Cui, L., Song, L., Yan, W., Li, Y., Lin, Z., Fang, H., 2018a. Study on the effects of natural gas hydrate cementation mode on the physical properties of rocks. J. Geophys. Eng. 15 (4), 1399–1406. https://doi.org/10.1088/1742-2140/aab625.
Dong, H., Sun, J., Lin, Z., Fang, H., Li, Y., Cui, L., Yan, W., 2018b. 3D pore-type digital rock modeling of natural gas hydrate for permafrost and numerical simulation of electrical properties. J. Geophys. Eng. 15 (1), 275–285. https://doi.org/10.1088/1742-2140/aa8a8e.
Doshi, H., Ray, A., Kothari, I., 2007. Bioremediation potential of live and dead Spirulina: spectroscopic, kinetics and SEM studies. Biotechnol. Bioeng. 96 (6), 1051–1063. https://doi.org/10.1002/bit.21190.
Dvorkin, J., Helgerud, M., Waite, W., Kirby, S., Nur, A., 2000. Introduction to physical properties and elasticity models. In: Max, M.D. (Ed.), Natural Gas Hydrate. Coastal Systems and Continental Margins. Springer, Dordrecht, pp. 245–260. https://doi.org/10.1007/978-94-011-4387-5_20.
Echlin, M., Burnett, T., Polonsky, A., Pollock, T., Withers, P., 2020. Serial sectioning in the SEM for three dimensional materials science. Curr. Opin. Solid State Mater. Sci. 24 (2), 100817. https://doi.org/10.1016/j.cossms.2020.100817.
English, N., MacElroy, J., 2015. Perspectives on molecular simulation of clathrate hydrates: progress, prospects and challenges. Chem. Eng. Sci. 121, 133–156. https://doi.org/10.1016/j.ces.2014.07.047.
English, N., Tse, J., 2010. Guest and host contributions towards thermal conduction in various polymorphs of methane hydrate. Comp. Mater. Sci. 49 (4), S176–S180. https://doi.org/10.1016/j.commatsci.2009.12.015.
English, N., Tse, J., Carey, D., 2009. Mechanisms for thermal conduction in various polymorphs of methane hydrate. Phys. Rev. B 80, 134306. https://doi.org/10.1103/PhysRevB.80.134306.
Falenty, A., Kuhs, W., Glockzin, M., Rehder, G., 2014. Self-preservation of CH_4 hydrates for gas transport technology: pressure-temperature dependence and ice microstructures. Energy Fuels 28 (10), 6275–6283. https://doi.org/10.1021/ef501409g.
Fan, Z., Sun, C., Kuang, Y., Wang, B., Zhao, J., Song, Y., 2017. MRI analysis for methane hydrate dissociation by depressurization and the concomitant ice generation. Energy Proc. 105, 4763–4768. https://doi.org/10.1016/j.egypro.2017.03.1038.
Fang, B., Ning, F., Ou, W., Wang, D., Zhang, Z., Yu, Y., Lu, H., Wu, J., Vlugt, T., 2019. The dynamic behavior of gas hydrate dissociation by heating in tight sandy reservoirs: a molecular dynamics simulation study. Fuel 258, 116106. https://doi.org/10.1016/j.fuel.2019.116106.
Freifeld, B., Kneafsey, T., 2004. Investigating methane hydrate in sediments using X-ray computed tomography. In: Taylor, C.E., Kwan, J.T. (Eds.), Advances in the Study of Gas Hydrates. Springer, Boston, pp. 227–238. https://doi.org/10.1007/0-306-48645-8_15.
Fukumoto, A., Kamada, K., Sato, T., Oyama, H., Torii, H., Kiyono, F., Nagao, J., Temma, N., Narita, H., 2017. Numerical simulation of pore-scale formation of methane hydrate in the sand sediment using the phase-field model. J. Nat. Gas Sci. Eng. 50, 269–281. https://doi.org/10.1016/j.jngse.2017.12.016.
Gajanayake, S., Gamage, R., Li, X., Huppert, H., 2023. Natural gas hydrates – insights into a paradigm-shifting energy resource. Energ. Rev. 2 (1), 100013. https://doi.org/10.1016/j.enrev.2022.100013.
Gao, Y., Chen, Y., Chen, L., Ji, G., Wang, K., Sun, B., 2019. Experimental investigation on the permeability of a hydrate-bearing reservoir considering overburden pressure. Fuel 246, 308–318. https://doi.org/10.1016/j.fuel.2019.01.166.
Garboczi, E., 1998. Finite element and finite difference programs for computing the linear electric and elastic properties of digital images of random materials. NIST Internal Report 6269. https://tsapps.nist.gov/publication/get_pdf.cfm?pub_id=860168.
Gerke, K., Vasilyev, R., Khirevich, S., Collins, D., Karsanina, M., Sizonenko, T., Korost, D., Lamontagne, S., Mallants, D., 2018. Finite-difference method Stokes solver (FDMSS) for 3D pore geometries: software development, validation and case studies. Comput. Geosci. 114, 41–58. https://doi.org/10.1016/j.cageo.2018.01.005.
Guo, Z., Lv, X., Liu, C., Chen, H., Cai, Z., 2022a. Characterizing gas hydrate–bearing marine sediments using elastic properties—Part 1: rock physical modeling and inversion from well logs. J. Mar. Sci. Eng. 10 (10), 1379. https://doi.org/10.3390/jmse10101379.
Guo, Z., Lv, X., Liu, C., Chen, H., Mei, L., 2022b. Characterizing gas hydrate-bearing marine sediments using elastic properties—Part 2: seismic inversion based on a pore-filling–solid matrix decoupling scheme. J. Mar. Sci. Eng. 10 (10), 1497. https://doi.org/10.3390/jmse10101497.
Guo, Z., Wang, X., Jiao, J., Chen, H., 2021. Rock physics model and seismic dispersion and attenuation in gas hydrate-bearing sediments. Front. Earth Sci. 9, 641606. https://doi.org/10.3389/feart.2021.641606.
He, G., Luo, X., Shakya, C., 2020. 2D investigation of water permeability in hydrate-bearing sediment with coexisting hydrate growth habits. J. Geophys. Eng. 17 (4), 563–576. https://doi.org/10.1093/jge/gxz120.
Hiruta, A., Matsumoto, R., 2022. Massive gas hydrates buried on Umitaka Spur in the Sea of Japan: description, origin, and significance to methane cycling in marine sediment. Geo Mar. Lett. 42 (3), 13. https://doi.org/10.1007/s00367-022-00735-w.
Holland, M., Schultheiss, P., 2014. Comparison of methane mass balance and X-ray computed tomographic methods for calculation of gas hydrate content of pressure cores. Mar. Petrol. Geol. 58, 168–177. https://doi.org/10.1016/j.marpetgeo.2014.07.016.
Hou, J., Ji, Y., Zhou, K., Liu, Y., Wei, B., 2018. Effect of hydrate on permeability in porous media: pore-scale micro-simulation. Int. J. Heat Mass Tran. 126, 416–424. https://doi.org/10.1016/j.ijheatmasstransfer.2018.05.156.
Hu, G., Li, C., Ye, Y., Liu, C., Zhang, J., Diao, S., 2014. Observation of gas hydrate distribution in sediment pore space. Chin. J. Geophys. 57 (5), 1675–1682. https://doi.org/10.6038/cjg20140530 (in Chinese).
Huang, X., Bandilla, K., Celia, M., 2015. Multi-physics pore-network modeling of two-phase shale matrix flows. Transport. Porous. Med 111, 123–141. https://doi.org/10.1007/s11242-015-0584-8.
Jang, J., Santamarina, J., 2011. Recoverable gas from hydrate-bearing sediments: pore network model simulation and macroscale analyses. J. Geophys. Res. 116, B08202. https://doi.org/10.1029/2010JB007841.
Ji, Y., Kneafsey, T., Hou, J., Zhao, J., Liu, C., Guo, T., Wei, B., Zhao, E., Bai, Y., 2022. Relative permeability of gas and water flow in hydrate-bearing porous media: a micro-scale study by lattice Boltzmann simulation. Fuel 321, 124013. https://doi.org/10.1016/j.fuel.2022.124013.
Jin, S., Nagao, J., Takeya, S., Jin, Y., Hayashi, J., Kamata, Y., Ebinuma, T., Narita, H., 2006. Structural investigation of methane hydrate sediments by microfocus X-ray computed tomography technique under high-pressure conditions. Jpn. J. Appl. Phys. 45, L714. https://doi.org/10.1143/JJAP.45.L714.
Ju, Y., Zheng, J., Epstein, M., Sudak, L.J., Wang, J., Zhao, X., 2014. 3D numerical reconstruction of well-connected porous structure of rock using fractal algorithms. Comput. Method. Appl. M. 279, 212–226. https://doi.org/10.1016/j.cma.2014.06.035.
Kang, D., Yun, T., Kim, K., Jang, J., 2016. Effect of hydrate nucleation mechanisms and capillarity on permeability reduction in granular media. Geophys. Res. Lett. 43 (17), 9018–9025. https://doi.org/10.1002/2016GL070511.
Kang, Q., Zhang, D., Lichtner, P., Tsimpanogiannis, I., 2004. Lattice Boltzmann model for crystal growth from supersaturated solution. Geophys. Res. Lett. 31, L21604. https://doi.org/10.1029/2004GL021107.
Katagiri, J., Konno, Y., Yoneda, J., Tenma, N., 2017. Pore-scale modeling of flow in particle packs containing grain-coating and pore-filling hydrates: verification of a Kozeny-Carman-based permeability reduction model. J. Nat. Gas Sci. Eng. 45, 537–551. https://doi.org/10.1016/j.jngse.2017.06.019.
Keehm, Y., Yoon, P., 2008. Pore-scale modeling of gas hydrate formation and comparison to lab experiments. In: SEG Las Vegas 2008 Annual Meeting. Las Vegas, Nevada, USA, pp. 1729–1733.
Kerkar, P., Horvat, K., Jones, K., Mahajan, D., 2014. Imaging methane hydrates growth dynamics in porous media using synchrotron X-ray computed microtomography. Geochem. Geophys. Geosy. 15 (12), 4759–4768. https://doi.org/10.1002/2014GC005373.
Kneafsey, T., Moridis, G., 2014. X-Ray computed tomography examination and comparison of gas hydrate dissociation in NGHP-01 expedition (India) and Mount Elbert (Alaska) sediment cores: experimental observations and numerical modeling. Mar. Petrol. Geol. 58, 526–539. https://doi.org/10.1016/j.marpetgeo.2014.06.016.
Kneafsey, T., Seol, Y., Gupta, A., Tomutsa, L., 2010. Permeability of laboratory-formed methane-hydrate-bearing sand: measurements and observations using X-Ray computed tomography. SPE J. 16 (1), 78–94. https://doi.org/10.2118/139525-PA.
Kneafsey, T., Tomutsa, L., Moridis, G., Seol, Y., Freifeld, B., Taylor, C., Gupta, A., 2007. Methane hydrate formation and dissociation in a partially saturated core-scale sand sample. J. Petrol. Sci. Eng. 56 (1–3), 108–126. https://doi.org/10.1016/j.petrol.2006.02.002.
Kondori, J., Zendehboudi, S., Hossain, M., 2017. A review on simulation of methane production from gas hydrate reservoirs: molecular dynamics prospective. J. Petrol. Sci. Eng. 159, 754–772. https://doi.org/10.1016/j.petrol.2017.09.073.
Kossel, E., Deusner, C., Bigalke, N., Haeckel, M., 2018. The dependence of water permeability in quartz sand on gas hydrate saturation in the pore space. J. Geophys. Res. 123 (2), 1235–1251. https://doi.org/10.1002/2017JB014630.
Kou, X., Li, X., Wang, Y., Wan, K., Chen, Z., 2021. Pore-scale analysis of relations between seepage characteristics and gas hydrate growth habit in porous sediments. Energy 218, 119503. https://doi.org/10.1016/j.energy.2020.119503.
Kuhs, W., Genov, G., Goreshnik, E., Zeller, A., Techmer, K., Bohrmann, G., 2004. The impact of porous microstructures of gas hydrates on their macroscopic properties. Int. J. Offshore Polar Eng. 14 (4), 305–309.
Kurihara, M., Sato, A., Funatsu, K., Ouchi, H., Masuda, Y., Narita, H., Collett, T., 2011. Analysis of formation pressure test results in the Mount Elbert methane hydrate reservoir through numerical simulation. Mar. Petrol. Geol. 28 (2), 502–516. https://doi.org/10.1016/j.marpetgeo.2010.01.007.
Kvamme, B., Graue, A., Aspenes, E., Kuznetsova, T., Gránásy, L., Tóth, G., Pusztai, T.,

Tegze, G., 2004. Kinetics of solid hydrate formation by carbon dioxide: phase field theory of hydrate nucleation and magnetic resonance imaging. Phys. Chem. Chem. Phys. 6 (9), 2327–2334. https://doi.org/10.1039/B311202K.
Kvenvolden, K., 1995. A review of the geochemistry of methane in natural gas hydrate. Org. Geochem. 23 (11–12), 997–1008. https://doi.org/10.1016/0146-6380(96)00002-2.
Lan, X., Zou, C., Peng, C., Wu, C., Zhang, Y., Wang, S., 2023. Numerical simulation of electrical properties for pore-scale hydrate-bearing sediments with different occurrence patterns and distribution morphologies. J. Mar. Sci. Eng. 11 (6), 1169. https://doi.org/10.3390/jmse11061169.
Le, T., Bornert, M., Brown, R., Aimedieu, P., Broseta, D., Chabot, B., King, A., Tang, A., 2021. Combining optical microscopy and X-ray computed tomography reveals novel morphologies and growth processes of methane hydrate in sand pores. Energies 14 (18), 5672. https://doi.org/10.3390/en14185672.
Lei, L., Liu, Z., Seol, Y., Boswell, R., Dai, S., 2019a. An investigation of hydrate formation in unsaturated sediments using X-ray computed tomography. J. Geophys. Res. 124 (4), 3335–3349. https://doi.org/10.1029/2018JB016125.
Lei, L., Park, T., Jarvis, K., Pan, L., Tepecik, I., Zhao, Y., Ge, Z., Choi, J., Gai, X., Galindo-Torres, S., Boswell, R., Dai, S., Seol, Y., 2022a. Pore-scale observations of natural hydrate-bearing sediments via pressure core sub-coring and micro-CT scanning. Sci. Rep. 12 (1), 3471. https://doi.org/10.1038/s41598-022-07184-6.
Lei, L., Seol, Y., Choi, J., Kneafsey, T., 2019b. Pore habit of methane hydrate and its evolution in sediment matrix – laboratory visualization with phase-contrast micro-CT. Mar. Petrol. Geol. 104, 451–467. https://doi.org/10.1016/j.marpetgeo.2019.04.004.
Lei, L., Seol, Y., Jarvis, K., 2018. Pore-scale visualization of methane hydrate-bearing sediments with micro-CT. Geophys. Res. Lett. 45 (11), 5417–5426. https://doi.org/10.1029/2018GL078507.
Lei, X., Yao, Y., Qin, X., Lu, C., Luo, W., Wen, Z., Yuan, X., 2022b. Pore structure changes induced by hydrate dissociation: an example of the unconsolidated clayey-silty hydrate bearing sediment reservoir in the South China Sea. Mar. Geol. 443, 106689. https://doi.org/10.1016/j.margeo.2021.106689.
Li, K., Chen, B., Yang, M., Song, Y., Sum, A., 2023c. Methane hydrate phase equilibrium considering dissolved methane concentrations and interfacial geometries from molecular simulations. J. Chem. Phys. 159, 244505. https://doi.org/10.1063/5.0174705.
Li, F., Sun, C., Li, S., Chen, G., Guo, X., Yang, L., Pan, H., Li, S., Zhang, K., 2012. Experimental studies on the evolvement of electrical resistivity during methane hydrate formation in sediments. Energy Fuels 26 (10), 6210–6217. https://doi.org/10.1021/ef301257z.
Li, R., Zhang, L., Zhou, J., Han, Z., Pan, Z., Schüttrumpf, H., 2023a. Investigation on permeability anisotropy in unconsolidated hydrate-bearing sediments based on pore-scale numerical simulation: effect of mineral particle shape and pore-filling. Energy 267, 126456. https://doi.org/10.1016/j.energy.2022.126456.
Li, R., Zhou, Y., Zhan, W., Yang, J., 2022. Pore-scale modelling of elastic properties in hydrate-bearing sediments using 4-D synchrotron radiation imaging. Mar. Petrol. Geol. 145, 105864. https://doi.org/10.1016/j.marpetgeo.2022.105864.
Li, X., Zhang, Y., Li, G., Chen, Z., Wu, H., 2011. Experimental investigation into the production behavior of methane hydrate in porous sediment by depressurization with a novel three-dimensional cubic hydrate simulator. Ind. Eng. Chem. Res. 25 (10), 4497–4505. https://doi.org/10.1021/ef200757g.
Li, Y., Ning, F., Xu, M., Qi, M., Sun, J., Nouri, A., Gao, D., Wu, N., 2023b. Experimental study on solid particle migration and production behaviors during marine natural gas hydrate dissociation by depressurization. Pet. Sci. 20 (6), 3610–3623. https://doi.org/10.1016/j.petsci.2023.05.018.
Li, Y., Xu, T., Xin, X., Xia, Y., Zhu, H., Yuan, Y., 2024. Multi-scale comprehensive study of the dynamic evolution of permeability during hydrate dissociation in clayey silt hydrate-bearing sediments. Adv. Geo-Energy Res. 12 (2), 127–140. https://doi.org/10.46690/ager.2024.05.05.
Li, Y., Yang, S., Wu, P., Song, X., Sun, X., 2021. Study of the physical characteristics of a pore-filling hydrate reservoir: particle shape effect. Energy Fuels 35 (19), 15502–15512. https://doi.org/10.1021/acs.energyfuels.1c01747.
Liang, H., Song, Y., Liu, Y., Yang, M., Huang, X., 2010. Study of the permeability characteristics of porous media with methane hydrate by pore network model. J. Nat. Gas Chem. 19 (3), 255–260. https://doi.org/10.1016/S1003-9953(09)60078-5.
Liang, J., Meng, M., Liang, J., Ren, J., He, Y., Li, T., Xu, M., Wang, X., 2022. Drilling cores and geophysical characteristics of gas hydrate-bearing sediments in the production test region in the Shenhu sea, South China sea. Front. Earth Sci. 10, 911123. https://doi.org/10.3389/feart.2022.911123.
Lin, Z., Dong, H., Pan, H., Sun, J., Fang, H., Wang, X., 2019. Study on the equivalence between gas hydrate digital rocks and hydrate rock physical models. J. Petrol. Sci. Eng. 181, 106241. https://doi.org/10.1016/j.petrol.2019.106241.
Liu, C., Meng, Q., Hu, G., Li, C., Sun, J., He, X., Wu, N., Yang, S., Liang, J., 2017a. Characterization of hydrate-bearing sediments recovered from the Shenhu area of the South China Sea. Interpret 5 (3), SM13–23. https://doi.org/10.1190/INT-2016-0211.1.
Liu, L., Lu, X., Zhang, X., Liu, C., Du, B., 2017b. Numerical simulations for analyzing deformation characteristics of hydrate-bearing sediments during depressurization. Adv. Geo-Energy Res. 1 (3), 135–147. https://doi.org/10.26804/ager.2017.03.01.
Liu, L., Zhang, Z., Li, C., Ning, F., Liu, C., Wu, N., Cai, J., 2020. Hydrate growth in quartzitic sands and implication of pore fractal characteristics to hydraulic, mechanical, and electrical properties of hydrate-bearing sediments. J. Nat. Gas Sci. Eng. 75, 103109. https://doi.org/10.1016/j.jngse.2019.103109.
Liu, S., Han, T., Fu, L., 2024. Distribution of gas hydrate in fractured reservoirs: implications from anisotropic elastic and electrical numerical simulations. Geophys. J. Int. 237 (2), 838–848. https://doi.org/10.1093/gji/ggae076.
Liu, X., Sun, J., Wang, H., 2009. Reconstruction of 3-D digital cores using a hybrid method. Appl. Geophys. 6, 105–112. https://doi.org/10.1007/s11770-009-0017-y.
Liu, Z., Kim, J., Lei, L., Ning, F., Dai, S., 2019. Tetrahydrofuran hydrate in clayey sediments—laboratory formation, morphology, and wave characterization. J. Geophys. Res. 124 (4), 3307–3319. https://doi.org/10.1029/2018JB017156.
Lu, C., Xia, Y., Qin, X., Ma, C., Bian, H., Xing, D., Lu, H., 2022. Micro- and nanoscale pore structure characterization and mineral composition analysis of clayey-silt hydrate reservoir in South China Sea. Geofluids 2022 (1), 2837193. https://doi.org/10.1155/2022/2837193.
MacDonald, G., 1990. The future of methane as an energy resource. Annu. Rev. Energ. 15, 53–83. https://doi.org/10.1146/annurev.eg.15.110190.000413.
Madhusudhan, B., Sahoo, S., Alvarez-Borges, F., Ahmed, S., North, L., Best, A., 2022. Gas bubble dynamics during methane hydrate formation and its influence on geophysical properties of sediment using high-resolution synchrotron imaging and rock physics modeling. Front. Earth Sci. 10, 877641. https://doi.org/10.3389/feart.2022.877641.
Mahabadi, N., Dai, S., Seol, Y., Jang, J., 2019. Impact of hydrate saturation on water permeability in hydrate-bearing sediments. J. Petrol. Sci. Eng. 174, 696–703. https://doi.org/10.1016/j.petrol.2018.11.084.
Mahabadi, N., Dai, S., Seol, Y., Yun, T., Jang, J., 2016. The water retention curve and relative permeability for gas production from hydrate-bearing sediments: pore-network model simulation. Geochem. Geophys. Geosy. 17 (8), 3099–3110. https://doi.org/10.1002/2016GC006372.
Mahabadi, N., Jang, J., 2014. Relative water and gas permeability for gas production from hydrate-bearing sediments. Geochem. Geophys. Geosy. 15 (6), 2346–2353. https://doi.org/10.1002/2014GC005331.
Majid, A., Koh, C., 2024. Applications of solid-state nuclear magnetic resonance (SS-NMR) for characterization of gas hydrates: a mini-review. Energy Fuels 38 (10), 8516–8527. https://doi.org/10.1021/acs.energyfuels.4c00487.
Miyoshi, T., Ohmura, R., Yasuoka, K., 2007. Predicting thermodynamic stability of clathrate hydrates based on molecular-dynamics simulations and its confirmation by phase-equilibrium measurements. J. Phys. Chem. C 111 (9), 3799–3802. https://doi.org/10.1021/jp068244e.
Mohammadmoradi, P., Kantzas, A., 2018. Direct geometrical simulation of pore space evolution through hydrate dissociation in methane hydrate reservoirs. Mar. Petrol. Geol. 89, 786–798. https://doi.org/10.1016/j.marpetgeo.2017.11.016.
Moon, C., Taylor, P., Rodger, P., 2003. Molecular dynamics study of gas hydrate formation. J. Am. Chem. Soc. 125 (16), 4706–4707. https://doi.org/10.1021/ja028537v.
Mork, M., Schei, G., Larsen, R., 2000. NMR imaging study of hydrates in sediments. Ann. NY. Acad. Sci. 912 (1), 897–905. https://doi.org/10.1111/j.1749-6632.2000.tb06843.x.
Moudrakovski, I., McLaurin, G., Ratcliffe, C., Ripmeester, J., 2004. Methane and carbon dioxide hydrate formation in water droplets: spatially resolved measurements from magnetic resonance microimaging. J. Phys. Chem. B 108 (45), 17591–17595. https://doi.org/10.1021/jp0473220.
Murshed, M., Klapp, S., Enzmann, F., Szeder, T., Huthwelker, T., Stampanoni, M., Marone, F., Hintermüller, C., Bohrmann, G., Kuhs, W., Kersten, M., 2008. Natural gas hydrate investigations by synchrotron radiation X-ray cryo-tomographic microscopy (SRXCTM). Geophys. Res. Lett. 35 (23), L23612. https://doi.org/10.1029/2008GL035460.
Nikitin, V., Dugarov, G., Duchkov, A., Fokin, M., Drobchik, A., Shevchenko, P., Carlo, F., Mokso, R., 2020. Dynamic in-situ imaging of methane hydrate formation and self-preservation in porous media. Mar. Petrol. Geol. 115, 104234. https://doi.org/10.48550/arXiv.1907.03052.
Øren, P., Bakke, S., 2002. Process based reconstruction of sandstones and prediction of transport properties. Transport. Porous. Med 46 (2), 311–343. https://doi.org/10.1023/A:1015031122338.
Orsi, T., Anderson, A., Leonard, J., Bryant, W., Edwards, C., 1992. Use of X-ray computed tomography in the study of marine sediments. In: Proceedings Civil Engineering in the Oceans V, College Station, Texas, USA, pp. 968–982.
Pan, L., Lei, L., Seol, Y., 2021. Pore-scale influence of methane hydrate on permeability of porous media. J. Nat. Gas Sci. Eng. 87, 103758. https://doi.org/10.1016/j.jngse.2020.103758.
Phan, A., Stamatakis, M., Koh, C., Striolo, A., 2023. Microscopic insights on clathrate hydrate growth from non-equilibrium molecular dynamics simulations. J. Colloid Interface Sci. 649, 185–193. https://doi.org/10.1016/j.jcis.2023.06.032.
Qian, Y., D'Humières, D., Lallemand, P., 1992. Lattice BGK models for Navier-Stokes equation. Europhys. Lett. 17 (6), 479–484. https://doi.org/10.1209/0295-5075/17/6/001.
Ramstad, T., Idowu, N., Nardi, C., Øren, P., 2012. Relative permeability calculations from two-phase flow simulations directly on digital images of porous rocks. Transport. Porous. Med 94 (2), 487–504. https://doi.org/10.1007/s11242-011-9877-8.
Roberts, A., Garboczi, E., 2002. Elastic properties of model random three-dimensional open-cell solids. J. Mech. Phys. Solids. 50 (1), 33–55. https://doi.org/10.1016/S0022-5096(01)00056-4.
Roberts, J., Schwartz, L., 1985. Grain consolidation and electrical conductivity in porous media. Phys. Rev. B 31 (9), 5990–5997. https://doi.org/10.1103/PhysRevB.31.5990.
Ruppel, C., Collett, T., 2013. Geological studies of methane hydrates reveal reserves

with potential. Energy Focus, 202–204.
Saenger, E., Enzmann, F., Keehm, Y., Steeb, H., 2011. Digital rock physics: effect of fluid viscosity on effective elastic properties. J. Appl. Geophys. 74 (4), 236–241. https://doi.org/10.1016/j.jappgeo.2011.06.001.
Sahoo, S., Madhusudhan, B., Marín-Moreno, H., North, L., Ahmed, S., Falcon-Suarez, I., Minshull, T., Best, A., 2018. Laboratory insights into the effect of sediment-hosted methane hydrate morphology on elastic wave velocity from time-lapse 4-D synchrotron X-Ray computed tomography. Geochem. Geophys. Geosy. 19 (11), 4502–4521. https://doi.org/10.1029/2018GC007710.
Sarupria, S., Debenedetti, P., 2011. Molecular dynamics study of carbon dioxide hydrate dissociation. J. Phys. Chem. A. 115 (23), 6102–6111. https://doi.org/10.1021/jp110868t.
Seol, Y., Kneafsey, T., 2009. X-ray computed-tomography observations of water flow through anisotropic methane hydrate-bearing sand. J. Petrol. Sci. Eng. 66 (3–4), 121–132. https://doi.org/10.1016/j.petrol.2009.01.008.
Shah, S., Crawshaw, J., Boek, E., 2014. Preparation of microporous rock samples for confocal laser scanning microscopy. Pet. Geosci. 20 (4), 369–374. https://doi.org/10.1144/petgeo2014-021.
Spangenberg, E., Kulenkampff, J., 2006. Influence of methane hydrate content on electrical sediment properties. Geophys. Res. Lett. 33 (24), L24315. https://doi.org/10.1029/2006GL028188.
Staykova, D., Kuhs, W., Salamatin, A., Hansen, T., 2003. Formation of porous gas hydrates from ice powders: diffraction experiments and multistage model. J. Phys. Chem. B 107 (37), 10299–10311. https://doi.org/10.1021/jp027787v.
Stern, L., Kirby, S., 2008. Natural gas hydrates up close: a comparison of grain characteristics of samples from marine and permafrost environments as revealed by cryogenic SEM. In: Proceedings of the 6th International Conference on Gas Hydrates (ICGH 2008), Vancouver, Canada. https://doi.org/10.14288/1.0041020.
Stern, L., Lorenson, T., 2014. Grain-scale imaging and compositional characterization of cryo-preserved India NGHP 01 gas-hydrate-bearing cores. Mar. Petrol. Geol. 58, 206–222. https://doi.org/10.1016/j.marpetgeo.2014.07.027.
Su, P., Lin, L., Lv, Y., Liang, J., Sun, Y., Wei, Z., He, H., Yan, B., Ji, Z., Wang, L., Wang, F., Cai, M., 2022. Potential and distribution of natural gas hydrate resources in the South China Sea. J. Mar. Sci. Eng. 10 (10), 1364. https://doi.org/10.3390/jmse10101364.
Sun, J., Li, C., Hao, X., Liu, C., Chen, Q., Wang, D., 2020. Study of the surface morphology of gas hydrate. J. Ocean. U. China. 19, 331–338. https://doi.org/10.1007/s11802-020-4039-7.
Sun, J., Zhang, Z., Wang, D., Liu, C., Lu, H., Song, K., 2021. Permeability change induced by dissociation of gas hydrate in sediments with different particle size distribution and initial brine saturation. Mar. Petrol. Geol. 123, 104749. https://doi.org/10.1016/j.marpetgeo.2020.104749.
Tahmasebi, P., Hezarkhani, A., Sahimi, M., 2012. Multiple-point geostatistical modeling based on the cross-correlation functions. Comput. Geosci. 16, 779–797. https://doi.org/10.1007/s10596-012-9287-1.
Talabi, O., Alsayari, S., Iglauer, S., Blunt, M., 2009. Pore-scale simulation of NMR response. J. Petrol. Sci. Eng. 67 (3–4), 168–178. https://doi.org/10.1016/j.petrol.2009.05.013.
Talukdar, M., Torsaeter, O., 2002. Reconstruction of chalk pore networks from 2D backscatter electron micrographs using a simulated annealing technique. J. Petrol. Sci. Eng. 33 (4), 265–282. https://doi.org/10.1016/S0920-4105(02)00148-1.
Tian, H., Liu, L., Zhu, L., Ge, X., Ding, P., Cai, J., 2023. Relationship between normalized permeability and resistivity index in hydrate-bearing sediments: fractal model and numerical simulation. Geophys. J. Int. 234 (1), 684–698. https://doi.org/10.1093/gji/ggad090.
Tian, H., Liu, W., Ding, P., Wei, W., Li, X., Cai, J., 2024. Numerical simulation of elastic properties of hydrate-bearing sediments with digital rock technology. Mar. Petrol. Geol. 160, 106592. https://doi.org/10.1016/j.marpetgeo.2023.106592.
Tomutsa, L., Silin, D., Radmilovic, V., 2007. Analysis of chalk petophysical properties by means of submicron-scale pore imaging and modeling. SPE. Reserv. Eval. Eng. 10 (3), 285–293. https://doi.org/10.2118/99558-PA.
Uchida, T., Dallimore, S., Mikammi, J., 2000. Occurrences of natural gas hydrates beneath the permafrost zone in Mackenzie Delta: visual and X-ray CT imagery. Ann. NY. Acad. Sci. 912 (1), 1021–1033. https://doi.org/10.1111/j.1749-6632.2000.tb06857.x.
Veesam, S., Ravipati, S., Punnathanam, S., 2019. Recent advances in thermodynamics and nucleation of gas hydrates using molecular modeling. Curr. Opin. Chem. Eng. 23, 14–20. https://doi.org/10.1016/j.coche.2019.01.003.
Waite, W., Santamarina, J., Cortes, D., Dugan, B., Espinoza, D., Germaine, J., Jang, J., Jung, J., Kneafsey, T., Shin, H., Soga, K., Winters, W., Yun, T., 2009. Physical properties of hydrate-bearing sediments. Rev. Geophys. 47 (4), RG4003. https://doi.org/10.1029/2008RG000279.
Wang, Y., Blunt, M., Armstrong, R., Mostaghimi, P., 2021. Deep learning in pore scale imaging and modeling. Earth Sci. Rev. 215, 103555. https://doi.org/10.1016/j.earscirev.2021.103555.
Wang, D., Wang, C., Li, C., Liu, C., Lu, H., Wu, N., Hu, G., Liu, L., Meng, Q., 2018a. Effect of gas hydrate formation and decomposition on flow properties of fine-grained quartz sand sediments using X-ray CT based pore network model simulation. Fuel 226, 516–526. https://doi.org/10.1016/j.fuel.2018.04.042.
Wang, J., Zhang, L., Zhao, J., Ai, L., Yang, L., 2018b. Variations in permeability along with interfacial tension in hydrate-bearing porous media. J. Nat. Gas Sci. Eng. 51, 141–146. https://doi.org/10.1016/j.jngse.2017.12.029.
Wang, J., Zhao, J., Yang, M., Li, Y., Liu, W., Song, Y., 2015a. Permeability of laboratory-formed porous media containing methane hydrate: observations using X-ray computed tomography and simulations with pore network models. Fuel 145, 170–179. https://doi.org/10.1016/j.fuel.2014.12.079.
Wang, J., Zhao, J., Zhang, Y., Wang, D., Li, Y., Song, Y., 2015b. Analysis of the influence of wettability on permeability in hydrate-bearing porous media using pore network models combined with computed tomography. J. Nat. Gas Sci. Eng. 26, 1372–1379. https://doi.org/10.1016/j.jngse.2015.08.021.
Wang, J., Zhao, J., Zhang, Y., Wang, D., Li, Y., Song, Y., 2016. Analysis of the effect of particle size on permeability in hydrate-bearing porous media using pore network models combined with CT. Fuel 163, 34–40. https://doi.org/10.1016/j.fuel.2015.09.044.
Wells, J., Chen, W., Hartman, R., Koh, C., 2021. Carbon dioxide hydrate in a microfluidic device: phase boundary and crystallization kinetics measurements with micro-Raman spectroscopy. J. Chem. Phys. 154, 114710. https://doi.org/10.1063/5.0039533.
Winters, W., Waite, W., Mason, D., Gilbert, L., Pecher, I., 2007. Methane gas hydrate effect on sediment acoustic and strength properties. J. Petrol. Sci. Eng. 56 (1–3), 127–135. https://doi.org/10.1016/j.petrol.2006.02.003.
Wu, N., Liu, C., Hao, X., 2018. Experimental simulations and methods for natural gas hydrate analysis in China. China. Geol. 1 (1), 61–71. https://doi.org/10.31035/cg2018008.
Wu, P., Li, Y., Sun, X., Liu, W., Song, Y., 2020. Pore-scale 3D morphological modeling and physical characterization of hydrate-bearing sediment based on computed tomography. J. Geophys. Res. 125 (12), e2020JB020570. https://doi.org/10.1029/2020JB020570.
Wu, Y., Tahmasebi, P., Liu, K., Lin, C., Kamrava, S., Liu, S., Fagbemi, S., Liu, C., Chai, R., An, S., 2023. Modeling the physical properties of hydrate-bearing sediments: considering the effects of occurrence patterns. Energy 278, 127674. https://doi.org/10.1016/j.energy.2023.127674.
Xiao, P., Li, J., Chen, W., Pang, W., Peng, X., Xie, Y., Wang, X., Deng, C., Sun, C., Liu, B., Zhu, Y., Peng, Y., Linga, P., Chen, G., 2023. Enhanced formation of methane hydrate from active ice with high gas uptake. Nat. Commun. 14 (1), 8068. https://doi.org/10.1038/s41467-023-43487-6.
Xing, L., Niu, J., Zhang, S., Cao, S., Wang, B., Lao, L., Wei, W., Han, W., Ge, X., Wei, Z., 2022. Experimental study on hydrate saturation evaluation based on complex electrical conductivity of porous media. J. Petrol. Sci. Eng. 208, 109539. https://doi.org/10.1016/j.petrol.2021.109539.
Xing, L., Qi, S., Xu, Y., Wang, B., Lao, L., Wei, W., Han, W., Wei, Z., Ge, X., Aliyu, A., 2021. Numerical study on complex conductivity characteristics of hydrate-bearing porous media. J. Nat. Gas Sci. Eng. 95, 104145. https://doi.org/10.1016/j.jngse.2021.104145.
Xu, J., Bu, Z., Qin, H., Li, S., Li, H., 2023. Pore-scale modeling of seepage behaviors and permeability evolution in heterogeneous hydrate-bearing sediments and its implications for the permeability model. Geoenerg. Sci. Eng. 221, 211372. https://doi.org/10.1016/j.geoen.2022.211372.
Xue, K., Zhao, J., Song, Y., Liu, W., Lam, W., Zhu, Y., Liu, Y., Cheng, C., Liu, D., 2012. Direct observation of THF hydrate formation in porous microstructure using magnetic resonance imaging. Energies 5 (4), 898–910. https://doi.org/10.3390/en5040898.
Yang, H., Xue, X., Chen, X., Xie, J., Zheng, Q., 2021. A study on the electrical characteristics of fractured gas hydrate reservoirs based on digital rock technology. Lithosphere 2021 (Special 4), 1365284. https://doi.org/10.2113/2021/1365284.
Yang, L., Falenty, A., Chaouachi, M., Haberthür, D., Kuhs, W., 2016. Synchrotron X-ray computed microtomography study on gas hydrate decomposition in a sedimentary matrix. Geochem. Geophys. Geosyst. 17 (9), 3717–3732. https://doi.org/10.1002/2016GC006521.
Yang, M., Chong, Z.R., Zheng, J., Song, Y., Linga, P., 2017. Advances in nuclear magnetic resonance (NMR) techniques for the investigation of clathrate hydrates. Renew. Sustain. Energy Rev. 74, 1346–1360. https://doi.org/10.1016/j.rser.2016.11.161.
Yang, Y., Yao, J., Wang, C., Gao, Y., Zhang, Q., An, S., Song, W., 2015. New pore space characterization method of shale matrix formation by considering organic and inorganic pores. J. Nat. Gas Sci. Eng. 27, 496–503. https://doi.org/10.1016/j.jngse.2015.08.017.
Yasuoka, K., Murakoshi, S., 2000. Molecular dynamics simulation of dissociation process for methane hydrate. Ann. Ny. Acad. Sci. 912, 678–684. https://doi.org/10.1111/j.1749-6632.2000.tb06823.x.
Yu, P., Sean, W., Yeh, R., Hsieh, L., Hsu, R., Sato, T., 2017. Direct numerical simulation of methane hydrate dissociation in pore-scale flow by using CFD method. Int. J. Heat Mass Tran. 113, 176–183. https://doi.org/10.1016/j.ijheatmasstransfer.2017.05.053.
Yuan, H., Han, D., Wang, Y., 2022. A review of rock physical models for elastic properties characterization of gas hydrate bearing sediments. J. Petrol. Sci. Eng. 218, 111013. https://doi.org/10.1016/j.petrol.2022.111013.
Yuan, H., Wang, Y., Wang, X., 2021. Seismic methods for exploration and exploitation of gas hydrate. J. Earth Sci. 32 (4), 839–849. https://doi.org/10.1007/s12583-021-1502-3.
Yuan, Q., Kong, L., Liang, Q., Liang, J., Yang, L., Dong, Y., Wang, Z., Wu, X., 2024. Mechanical characteristics of gas hydrate-bearing sediments: an experimental study from the South China Sea. J. Mar. Sci. Eng. 12 (2), 301. https://doi.org/10.3390/jmse12020301.
Yun, T., Lee, C., Lee, J., Bahk, J., Santamarina, J., 2011. A pressure core based characterization of hydrate-bearing sediments in the Ulleung Basin, Sea of Japan (East Sea). J. Geophys. Res. 116 (B2), B02204. https://doi.org/10.1029/2010JB007468.

Zhang, Y., Zhao, J., Bhattacharjee, G., Xu, H., Yang, M., Kumar, R., Linga, P., 2022c. Synthesis of methane hydrate at ambient temperature with ultra-rapid formation and high gas storage capacity. Energy Environ. Sci. 15 (12), 5362–5378. https://doi.org/10.1039/D2EE01968J.

Zhang, Y., Zhao, L., Deng, S., Nie, X., Du, Z., 2019c. Molecular dynamics simulation on carbon dioxide hydrate formation. Energy Proc. 158, 4648–4654. https://doi.org/10.1016/j.egypro.2019.01.741.

Zhang, Z., Wu, N., Liu, C., Hao, X., Zhang, Y., Gao, K., Peng, B., Zheng, C., Tang, W., Guo, G., 2022d. Molecular simulation studies on natural gas hydrate nucleation and growth: a review. China Geol 5 (2), 330–344. https://doi.org/10.31035/cg2022017.

Zhang, B., Yu, C., Fan, G., Sun, Y., Li, J., 2022a. Application of high-precision 3D seismics for gas hydrate exploration in Muli area of Qinghai Province, China—a case study. Arab. J. Geosci. 15 (14), 1276. https://doi.org/10.1007/s12517-022-10545-0.

Zhang, J., Liu, X., Chen, D., Yin, Z., 2022b. An investigation on the permeability of hydrate-bearing sediments based on pore-scale CFD simulation. Int. J. Heat Mass Tran. 192, 122901. https://doi.org/10.1016/j.ijheatmasstransfer.2022.122901.

Zhang, L., Sun, L., Sun, M., Lv, X., Dong, H., Miao, Y., Yang, L., Song, Y., Zhao, J., 2019a. Analyzing spatially and temporally visualized formation behavior of methane hydrate in unconsolidated porous media. Magn. Reson. Imaging 61, 224–230. https://doi.org/10.1016/j.mri.2019.06.005.

Zhang, L., Sun, M., Sun, L., Yu, T., Song, Y., Zhao, J., Yang, L., Dong, H., 2020. In-situ observation for natural gas hydrate in porous medium: water performance and formation characteristic. Magn. Reson. Imaging 65, 166–174. https://doi.org/10.1016/j.mri.2019.09.002.

Zhang, L., Zhang, C., Zhang, K., Zhang, L., Yao, J., Sun, H., Yang, Y., 2019b. Pore-scale investigation of methane hydrate dissociation using the lattice Boltzmann method. Water Resour. Res. 55 (11), 8422–8444. https://doi.org/10.1029/2019WR025195.

Zhang, X., Du, Z., Luan, Z., Wang, X., Xi, S., Wang, B., Li, L., Lian, C., Yan, J., 2017. In situ Raman detection of gas hydrates exposed on the seafloor of the South China Sea. Geochem. Geophys. Geosy. 18 (10), 3700–3713. https://doi.org/10.1002/2017GC006987.

Zhao, G., Yang, M., Lv, X., Zheng, J., Song, Y., 2023a. MRI insight on multiphase flow in hydrate-bearing sediment and development mechanism of hydrate seal. Pet. Sci. 20 (6), 3854–3864. https://doi.org/10.1016/j.petsci.2023.07.017.

Zhao, J., Shi, Z., Li, Y., Xiang, X., Li, J., Wei, N., 2021. Simulation of conductivity characteristics of gas hydrate reservoirs and its saturation calculation. Nat. Gas Geosci. 32 (9), 1261–1269. https://doi.org/10.11764/j.issn.1672-1926.2021.03.003 (in Chinese).

Zhao, J., Sun, J., Liu, X., Chen, H., Cui, L., 2013. Numerical simulation of the electrical properties of fractured rock based on digital rock technology. J. Geophys. Eng. 10 (5), 055009. https://doi.org/10.1088/1742-2132/10/5/055009.

Zhao, J., Yao, L., Song, Y., Xue, K., Cheng, C., Liu, Y., Zhang, Y., 2011. In situ observations by magnetic resonance imaging for formation and dissociation of tetrahydrofuran hydrate in porous media. Magn. Reson. Imaging 29 (2), 281–288. https://doi.org/10.1016/j.mri.2010.08.012.

Zhao, Y., Liu, J., Sang, S., Hua, L., Kong, L., Zeng, Z., Yuan, Q., 2023b. Experimental investigation on the permeability characteristics of methane hydrate-bearing clayey-silty sediments considering various factors. Energy 269, 126811. https://doi.org/10.1016/j.energy.2023.126811.

Zhu, L., Zhang, C., Zhang, C., Zhou, X., Zhang, Z., Nie, X., Liu, W., Zhu, B., 2019. Challenges and prospects of digital core-reconstruction research. Geofluids 2019 (1), 7814180. https://doi.org/10.1155/2019/7814180.

Zhu, Y., Wang, P., Pang, S., Zhang, S., Xiao, R., 2021. A review of the resource and test production of natural gas hydrates in China. Energy Fuels 35 (11), 9137–9150. https://doi.org/10.1021/acs.energyfuels.1c00485.